Chapter 1

Ferromagnetic Shape Memory Alloys: Foams and Microwires

Xuexi Zhang and Mingfang Qian

Additional information is available at the end of the chapter

http://dx.doi.org/10.5772/intechopen.69702

Abstract

Ferromagnetic shape memory alloys exhibit martensite transformation (MT) and magnetic transition and thus may be actuated by thermal and magnetic fields. The working frequency of these alloys may be higher than conventional shape memory alloys, such as Ni-Ti, because the magnetic field may operate at higher frequency. This chapter focuses on some fundamental topics of these multifunctional materials, including the composition-structure relationship, the synthesis of the foams and microwires, the martensite transformation and magnetic transition characters, the properties (magnetic-field-induced strain (MFIS), magnetocaloric effects (MCEs), shape memory effects, and superelastic effects), and applications. The improvement of the magnetic-field-induced strain due to the reduced constraint of twin boundary motion caused by grain boundaries in polycrystalline Ni-Mn-Ga foams and the size effects of the superelasticity and magnetocaloric properties in Ni-Mn-X (X = In, Sn, Sb) microwires are detailed and addressed.

Keywords: ferromagnetic shape memory alloys (FSMAs), Ni-Mn-Ga alloys, foams, microwires, martensite transformation, ferromagnetic-field-induced strain (MFIS), magnetocaloric effects (MCEs)

1. Introduction

Ferromagnetic shape memory Heusler alloys, such as Ni-Mn-Ga and Ni-Mn-X (X = In, Sn, Sb), are receiving increasing attentions due to their multifunctional properties, that is, magnetic-field-induced strain (MFIS), magnetocaloric effect (MCE), magnetoresistance, etc. Before 1996, some works concern the martensite transformation (MT) of Ni-Mn-Ga alloys [1–3]. The relationship between the composition on martensite and magnetic transformation temperatures has also been revealed [4]. In 1996, Ullakko et al. published the first paper on the MFIS

of single-crystalline Ni-Mn-Ga alloys [5]. Since then, high MFIS of 6.4% has been found in Ni-Mn-Ga alloys with 5M martensite structure [6] and of 10% with 5M martensite structure [7]. By allying a high magnetic field, the single-crystalline Ni-Mn-Ga alloy with non-modulate (NM) martensite structure may show a giant MFIS as high as 12% [8]. In 2007, Müllner et al. published their first paper on Ni-Mn-Ga foam and found that 0.24% MFIS may be achieved in the foams with single-model pore architecture [9]. By introducing secondary pores, thus forming dual-pore architecture, the foams may exhibit a MFIS of 8.7% after suitable thermal-magnetic training, which approaches the theoretical limit of single-crystalline Ni-Mn-Ga alloys with 14M martensite structure [10]. In 2008, Scheerbaum et al. [11] produced Ni-Mn-Ga fibers with diameter ~60–100 μm, which showed a 1% MFIS upon applying an external magnetic field of 2 T. Since 2012, researchers in Harbin Institute of Technology make use of the so-called melt extraction method to fabricate microwires on a large quantity [12, 13]. The obtained microwire has a naked surface, which can be directly used in MEMS or NEMS, and acts as building blocks for composites and complex-shaped components. Systematic research works have also been carried out to reveal the superelasticity [14, 15], shape memory [12, 16], and MCE properties [17–19].

Ni-Mn-X (X = In, Sn, Sb) alloys, another important ferromagnetic shape memory alloy family, attracted attention of the scientific society since Kainuma et al. [20] reported the giant stress output in Ni-Mn-In-Co alloys. On contrary to Ni-Mn-Ga alloys, these Ni-Mn-X alloys exhibit paramagnetic/antiferromagnetic martensite and ferromagnetic austenite. As a result, a bias magnetic field may stabilize the austenite phase, which is responsible for the shift of martensite transformation temperatures to lower temperature. Such metamagnetic structural transition from the paramagnetic/antiferromagnetic martensite to ferromagnetic austenite under a bias magnetic field may produce giant MCE [21].

This chapter describes the synthesis, processing, and properties (especially the MIFS and MCE) of these alloys, with emphasis on Ni-Mn-Ga foams and microwires. The up-to-date results, mainly reported in the past decades, will be covered. The aim of this chapter is to provide researchers an overview of the background, current status, and future development of the ferromagnetic shape memory alloys.

2. Composition-structure relationship in ferromagnetic shape memory alloys

2.1. Relationship between composition (*e*/*a*) and transformation temperatures

Off-stoichiometric Ni-Mn-Ga ferromagnetic shape memory alloys (FSMAs) have been attracted much attention because of their multiplicity of functional properties like excellent magnetic-field-induced strains (MFIS) [6, 7, 10], magnetocaloric effect (MCE) [22–24], conventional/magnetic shape memory effects (SME) [12], etc. The martensite phase or the martensite transformation (MT) temperatures (martensite start and finish temperature M_s, M_f, and the austenite start and finish temperature A_s, A_f) of the alloys are closely related to their functional properties. For instance, the Ni-Mn-Ga alloys show MFIS only in the martensitic state owing

to the reorientation of the twin boundaries in an applied magnetic field. As for the MCE, the effective refrigeration working temperature interval (WTI) of the cooling system is within the MT range. For Ni-Mn-Ga alloys, the MT temperatures of the alloy are particularly sensitive to their compositions [4].

Here, we focused our content on Ni-Mn-Ga alloys due to the space limit. For the stoichiometric Ni_2MnGa, the MT temperatures are lower than room temperature (RT), ~185 K; thus, no martensite exists at RT. By varying the composition of 5 at.%, a huge M_s change from 154 to 458 K can be obtained [4, 25–30]. The effect of composition on MT temperatures of the Ni-Mn-Ga alloys was studied by Chernenko et al. at 1995 [4]. A general view of transformation temperature shifting as a function of the Ni/Mn/Ga element content was summarized as (1) at a constant value of Mn content, Ga addition lowers M_s temperature, (2) Mn addition (instead of Ga) at constant Ni concentration increases M_s, and (3) substitution of Ni atoms by Mn at constant Ga content results in alloys with lower M_s.

Furthermore, based on the M_s and transformation enthalpy (ΔH), Ni-Mn-Ga alloys were classified into three groups, as demonstrated in **Table 1** [4, 31, 32], where T_c stands for the magnetic transformation of Curie temperature of the alloy.

Thereafter, more systematic and quantized studies have been performed [25–30]. The effects of composition on temperature and ΔH can be formulated by the linear regression listed as follows [30]:

$$M_s\ (\mathrm{K}) = 25.44\mathrm{Ni}\ (\mathrm{at.\%}) - 4.86\mathrm{Mn}\ (\mathrm{at.\%}) - 38.83\mathrm{Ga}\ (\mathrm{at.\%}) \tag{1}$$

$$\Delta H\ (\mathrm{J/g}) = 0.72\mathrm{Ni}\ (\mathrm{at.\%}) - 0.16\mathrm{Mn}\ (\mathrm{at.\%}) - 1.23\mathrm{Ga}\ (\mathrm{at.\%}) \tag{2}$$

The number of valence electrons per atom (e/a) for Ni, Mn, and Ga atoms is $10(3d^{9.9}4s^{0.1})$, $7(3d^5 4s^2)$, and $10(4s^2 4p^1)$, respectively [26]; thus, the valence electron concentration of the alloy can be defined as

$$e/a = \frac{10\,\mathrm{Ni}_{at\%} + 7\,\mathrm{Mn}_{at\%} + 3\,\mathrm{Ga}_{at\%}}{\mathrm{Ni}_{at\%} + \mathrm{Mn}_{at\%} + \mathrm{Ga}_{at\%}} \tag{3}$$

The relationship between M_s temperature and e/a is summarized and presented in **Figure 1**. Statistical analysis shows a relatively large standard deviation of 44.7 K and a maximum error of 140.2 K for the extreme case, which implies that the MT may also be very sensitive to the microstructure of the alloy, that is, internal stress and the degree of the atomic order [14].

Group	e/a	M_s (T)	ΔH (J/g)
Group I	<7.7	$M_s < \mathrm{RT} < T_c$	~1.6
Group II	7.55–7.7	$M_s \approx \mathrm{RT} < T_c$	~4.2
Group III	>7.7	$M_s > T_c$	~8.5

Table 1. Classification of Ni-Mn-Ga alloys according to M_s and enthalpy (ΔH) [4, 17].

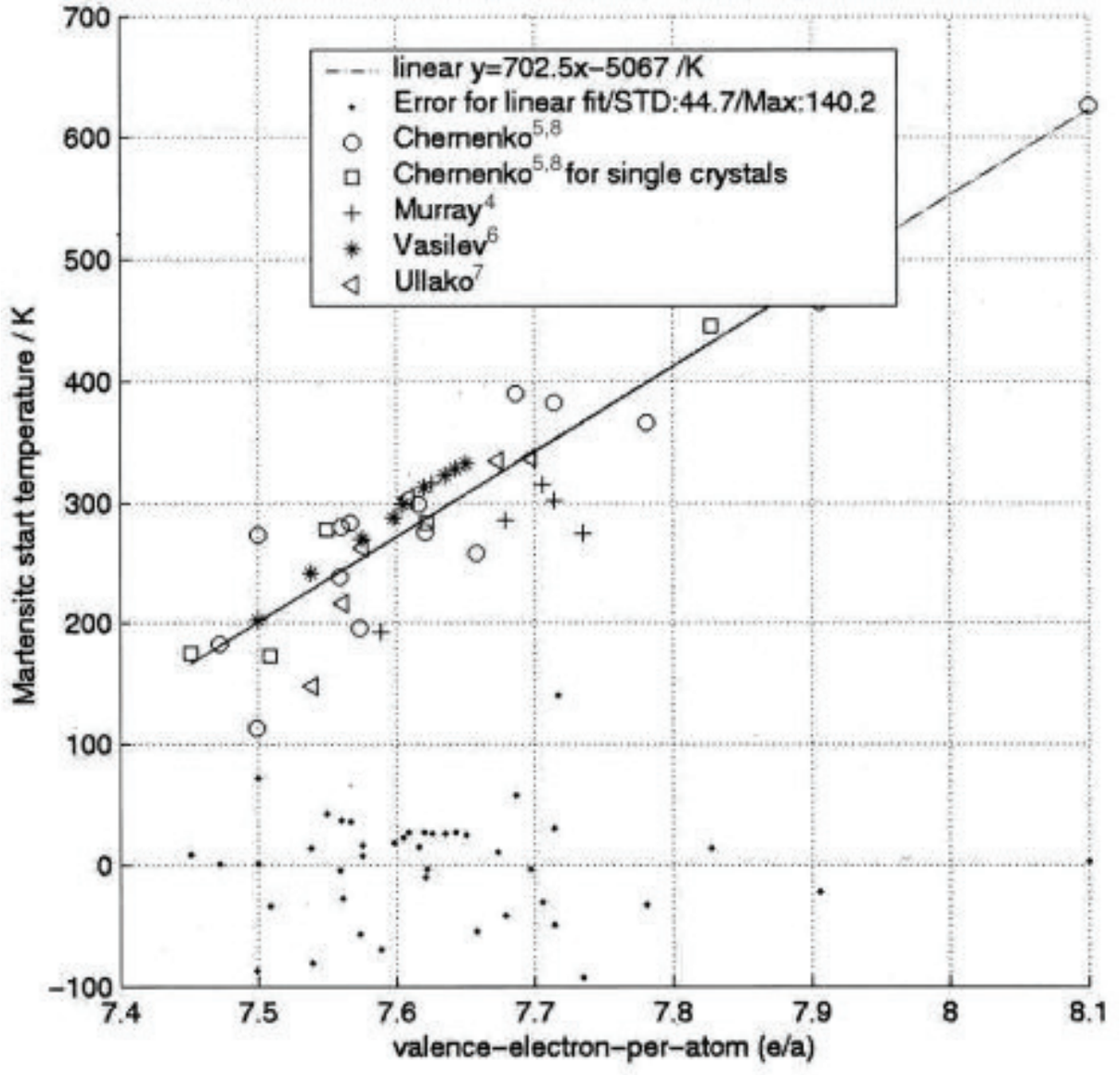

Figure 1. The relationship between martensite transformation temperatures and valence electron concentration of Ni-Mn-Ga alloy [29].

Based on **Figure 1**, the effects of e/a on M_s temperature can be formulated by the linear regression, as listed in Eq. (4), indicating that the MT temperature increases with increasing e/a:

$$M_s = 702.5(e/a) - 5067 \tag{4}$$

Besides, T_c varies less with composition variation (Mn, 20–35 at.%; Ga, 16–17 at.%) than M_s for Ni-Mn-Ga alloys [17, 29]. The effect of composition on the T_c of Ni-Mn-Ga alloy mainly relies on the Mn-Mn distance since the ferromagnetism mainly depends on the Mn-Mn atomic interaction [33]. The stoichiometric Ni_2MnGa alloy possesses the strongest ferromagnetic interaction between the neighboring Mn-Mn atoms with T_c ~ 376 K. Either with the concentration or expansion of the unit cell, the Mn-Mn nearest distance may be decreased; thus, the ferromagnetic interaction between neighboring Mn-Mn atoms can be weakened, which gives rise to a slight decrease of T_c [34].

Above all, the tunable transformation temperatures lead to multifunctional properties in Ni-Mn-Ga alloys, which will be demonstrated in details in Section 5.

2.2. Phase and structure of the martensite

Ni-Mn-Ga alloys exhibit a chemical ordering transition (a kind of second-order phase transition) from partially ordered high-temperature B2 phase to chemical ordered $L2_1$ phase during cooling. In the $L2_1$ phase, the Ni, Mn, and Ga atoms occupy the specific sites of the crystal lattice, as shown in **Figure 2**.

The $L2_1$ phase has a cubic face-centered lattice. On the other hand, Ni_2MnGa alloy displays martensite transformation (a kind of first-order phase transition). The martensite phase may show various stacking sequences, that is, a modulate structure, which thus creates martensite structure, such as five-layer modulate (5M) martensite phase (**Figure 3**), seven-layer modulate martensite phase (7M, **Figure 4**), and non-modulate (NM) martensite phase (**Figure 5**). The kind of modulation mainly depends on the composition of the alloy. These different martensite structures exhibit different twinning stresses, which has a large effect on the magnetic-field-induced strain and will be summarized in detail in Section 5.1.2.

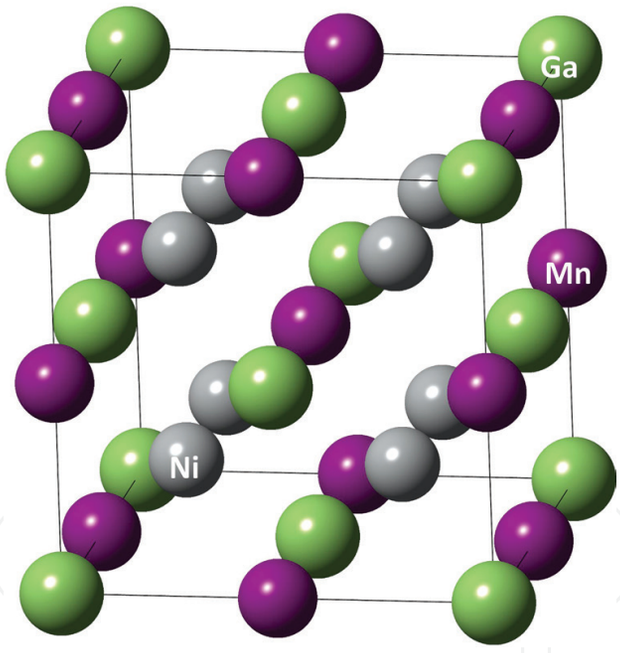

Figure 2. $L2_1$ crystal structure of the Ni_2MnGa alloys.

3. Synthesis of ferromagnetic Ni-Mn-Ga foams and microwires

3.1. Ni-Mn-Ga foams

Ferromagnetic Ni-Mn-Ga foams can produce large magnetic-field-induced strain of ~2.0–8.7% due to the reduction of constraints imposed by grain boundaries and the formation of bamboo

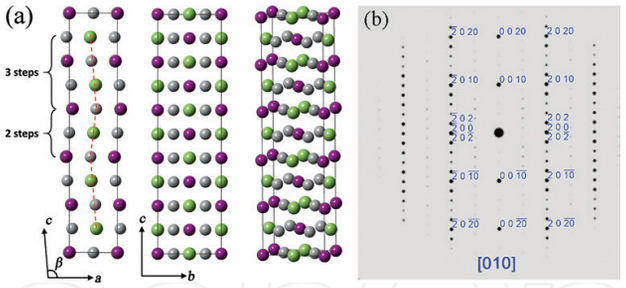

Figure 3. (a) 5M crystal structure of the Ni_2MnGa alloys and (b) simulated diffraction pattern of 5M martensite along crystal zone axis of [0 1 0].

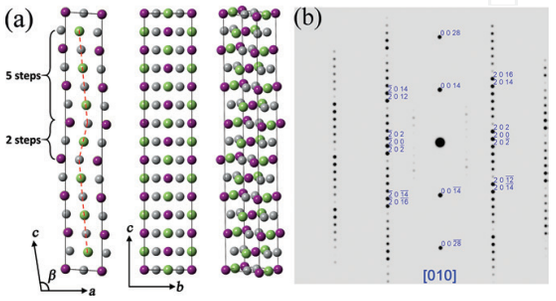

Figure 4. (a) 7M crystal structure of the Ni_2MnGa alloys and (b) simulated diffraction pattern of 7M martensite along crystal zone axis of [0 1 0].

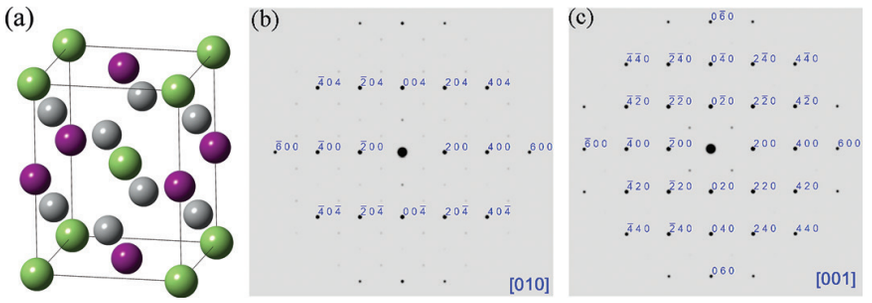

Figure 5. (a) NM crystal structure of the Ni_2MnGa alloys and simulated diffraction pattern of NM martensite along crystal zone axis of (b) [0 1 0] and (c) [0 0 1].

grains in the struts [10]. In this section, the synthesis of the Ni-Mn-Ga foams with single-pore and dual-pore distribution is demonstrated in detail [9, 35].

The casting replication method, that is, using liquid metal infiltration of a preform of ceramic space holder powder [36, 37], was used to prepare the Ni-Mn-Ga foams. Sodium aluminate ($NaAlO_2$) was used as space holder in this case due to its high melting temperature ~1650°C, excellent chemical stability with molten metals, and good solubility in acid. In order to create the single-pore and dual-pore distribution, different sizes of $NaAlO_2$ powders were prepared as follows: (1) purchased $NaAlO_2$ powders was cold pressed at 125 MPa and sintered at 1500°C for 3 h in the air; (2) the sintered body was broken up with a mortar and pestle into powders; and (3) the resulting powder was sieved into different size ranges: R1 for single-pore foam and R2 (coarse) and R3 (fine) for dual-pore foam. The specific size of the powder was tuned due to the requirement of the foam porosity.

For single-pore specimen, the R1 powder was directly poured into an alumina crucible and slightly trapped to the designed height. For dual-pore specimen, the coarse and fine powders were poured alternatively (layer by layer) in the crucible filled with acetone: the coarse powder was first poured in a small batch, followed by a small batch of fine powder to settle in the space between the coarse ones of the previous batch. After that, the crucible was heated to evaporate the acetone. Both crucibles were heated at 1500°C for 3 h in the air to create necks between powders for the infiltration of the Ni-Mn-Ga liquid metal and the formation of open pores.

For infiltration process, the ingot was placed on top of the sintered powder preform and then heated to melt the Ni-Mn-Ga alloy under vacuum in the furnace. After melting the alloy, high-purity Ar gas was introduced in the furnace at a pressure of 1.34 atm. to squeeze the molten alloy into the preform, and the temperature was then cooled to room temperature at 7°C/min.

The removal of the $NaAlO_2$ is critical for the preparation of the Ni-Mn-Ga foams. For the single-pore foam, a 10% HCl solution was used. Ten percent of HCl solution not only solve the $NaAlO_2$ but also solve the Ni-Mn-Ga alloy, thus, thinned the struts. In this case, for the dual-pore foam, the thin struts around the fine powders would be dissolved after long exposure to the 10% HCl solution. Thus, a two-step method was applied: (1) removal of the coarse powders without alloy dissolution and (2) removal of the remaining fine powders as well as some thinning of the alloy. The acid for the first step should dissolve $NaAlO_2$ but not the alloy. The acid for the second step should rapidly dissolve $NaAlO_2$ while slowly dissolving the alloy only to open small fenestrations between the fine $NaAlO_2$ powders. The mass loss of the bulk nonporous Ni-Mn-Ga alloy vs. time plots is shown in **Figure 6a**, which are linear for the acids of 10% HCl, 20% HCl, and 34% H_2SO_4. The slopes corresponding to dissolution rates are 16 and 5 mg/m^2 min in 10% HCl and 34% H_2SO_4, respectively, while triple the rate when doubled the concentration to 20% HCl.

As a result, 34% H_2SO_4 and 10% HCl were selected for the two steps, respectively. **Figure 6b** plots the mass loss vs. time for a foam sample with dual-size $NaAlO_2$ powder immersed in 34% H_2SO_4. After 2000 min, only 87% of the $NaAlO_2$ was removed from the sample. Thereafter, a similar foam sample was firstly immersed in a 34% H_2SO_4 solution for 645 min (corresponding

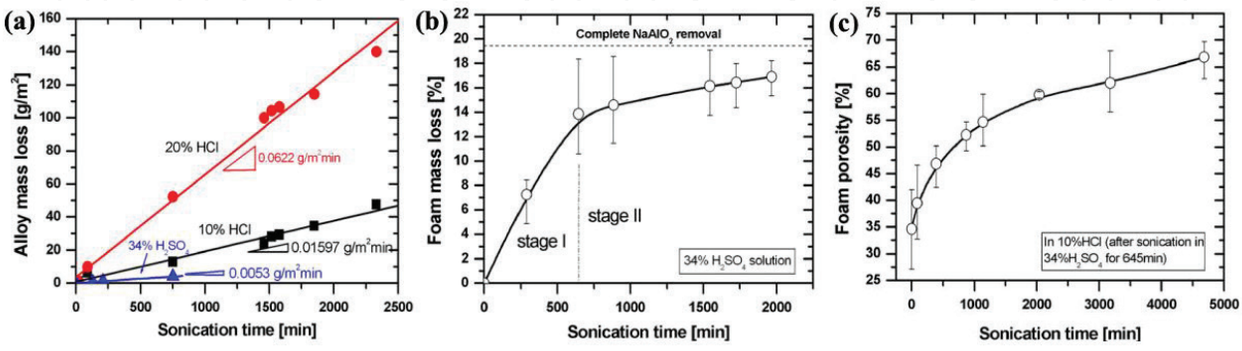

Figure 6. (a) Plot of mass loss vs. time in bulk Ni-Mn-Ga alloy immersed in 10% HCl, 20% HCl, and 34% H_2SO_4; (b) plot of mass loss vs. time for foam with dual-size $NaAlO_2$ powders in 34% H_2SO_4; and (c) plot of foam porosity vs. time for foam with dual-size $NaAlO_2$ powders immersed in 10% HCl after 645 min in 34% H_2SO_4 [35].

to the rapid dissolution stage in **Figure 6b**) and then transferred to the 10% HCl solution. A porosity of 55% was measured after 1140 min in 10% HCl, which was higher than the original $NaAlO_2$ fraction of 45%, indicating the full removal of the $NaAlO_2$ and partial dissolve of the alloy, as shown in **Figure 6c**. Further immersion increased the porosity due to the dissolve of the alloy only.

The morphologies of the fabricated single-pore and dual-pore foams are presented in **Figures 7** and **8**. In foams containing dual pores (**Figure 7b**), the alloy between large pores, which is solid in the single-pore foams (**Figure 7a**), contains small pores, thus producing many small nodes and struts. The three-dimensional architecture of both foams can be seen more vivid in **Figure 8**.

3.2. Ni-Mn-Ga microwires

Metallic microwires can be produced by a variety of methods, that is, melt extraction, Taylor method, melt-spinning, in-rotating water spinning, etc. Details of the fabrication method regarding the fabrication of ferromagnetic wires have been demonstrated by Peng et al. [38]. In recent years, the Taylor-Ulitovsky method was widely used for many metals and alloys. In this process, a metallic ingot is put in a glass tube and melted by induction heating. The glass tube was chosen to have relatively higher melting point than the ingot. Then, the glass tube is softened due to its contact with the molten metal, and it can be drawn. Recently, this method has been modified and applied to create glass-coated Ni-Mn-Ga microwires with equiaxed cross section, as shown in **Figure 9** [39, 40].

In the meantime, melt extraction has been established as a cost-effective and highly efficient method for the production of intrinsically brittle Ni-Mn-Ga alloys on a large scale [13]. The rapid solidification rate during melt extraction is suitable for obtaining refined microstructure, extended elemental solubility, and reduced elemental segregation [41].

A schematic melt extraction facility is displayed in **Figure 10a**. The microwire preparation process consists of the following steps: (1) the Ni-Mn-Ga ingot was inserted into a ceramic

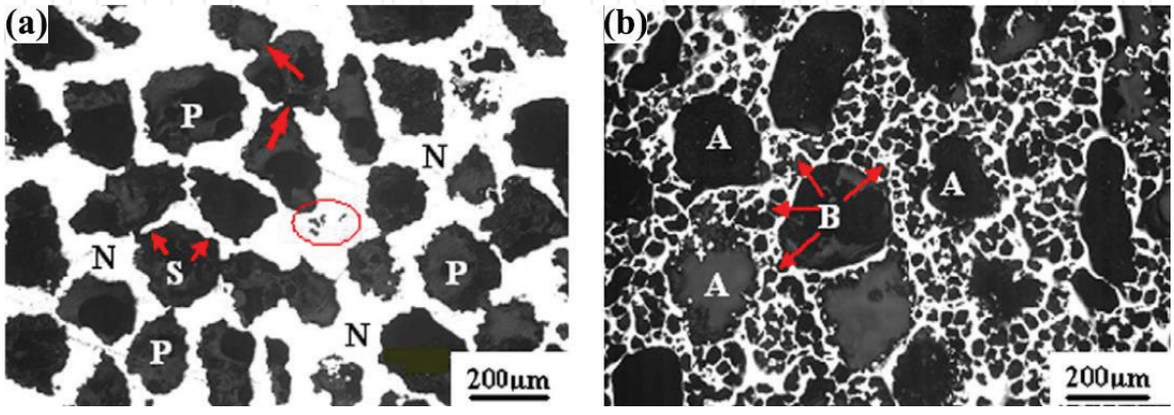

Figure 7. Optical micrographs of polished cross section of Ni-Mn-Ga foams. Metal struts (S) and nodes (N) appear bright, and the pores appear dark. Foams with (a) single and (b) dual-pore size distribution are presented [35].

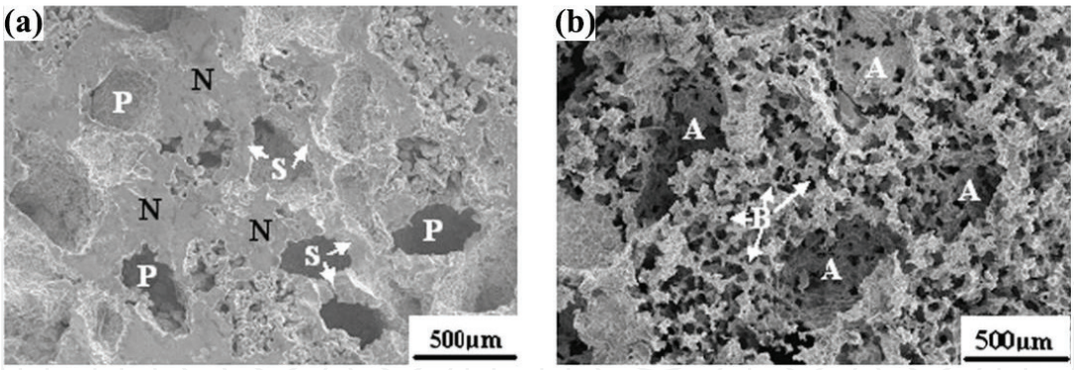

Figure 8. SEM micrographs of cut and etched surface of Ni-Mn-Ga foams showing three-dimensional structure and connectivity of pores. (a) Single- and (b) dual-pore foams are presented [35].

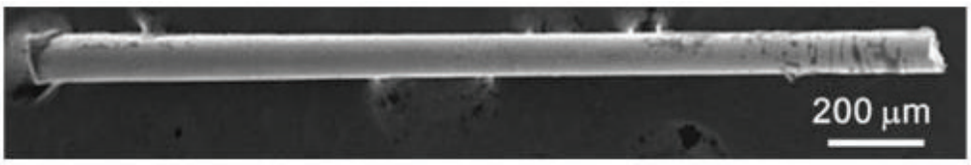

Figure 9. SEM image of representative Ni-Mn-Ga microwires created by the Taylor method [40].

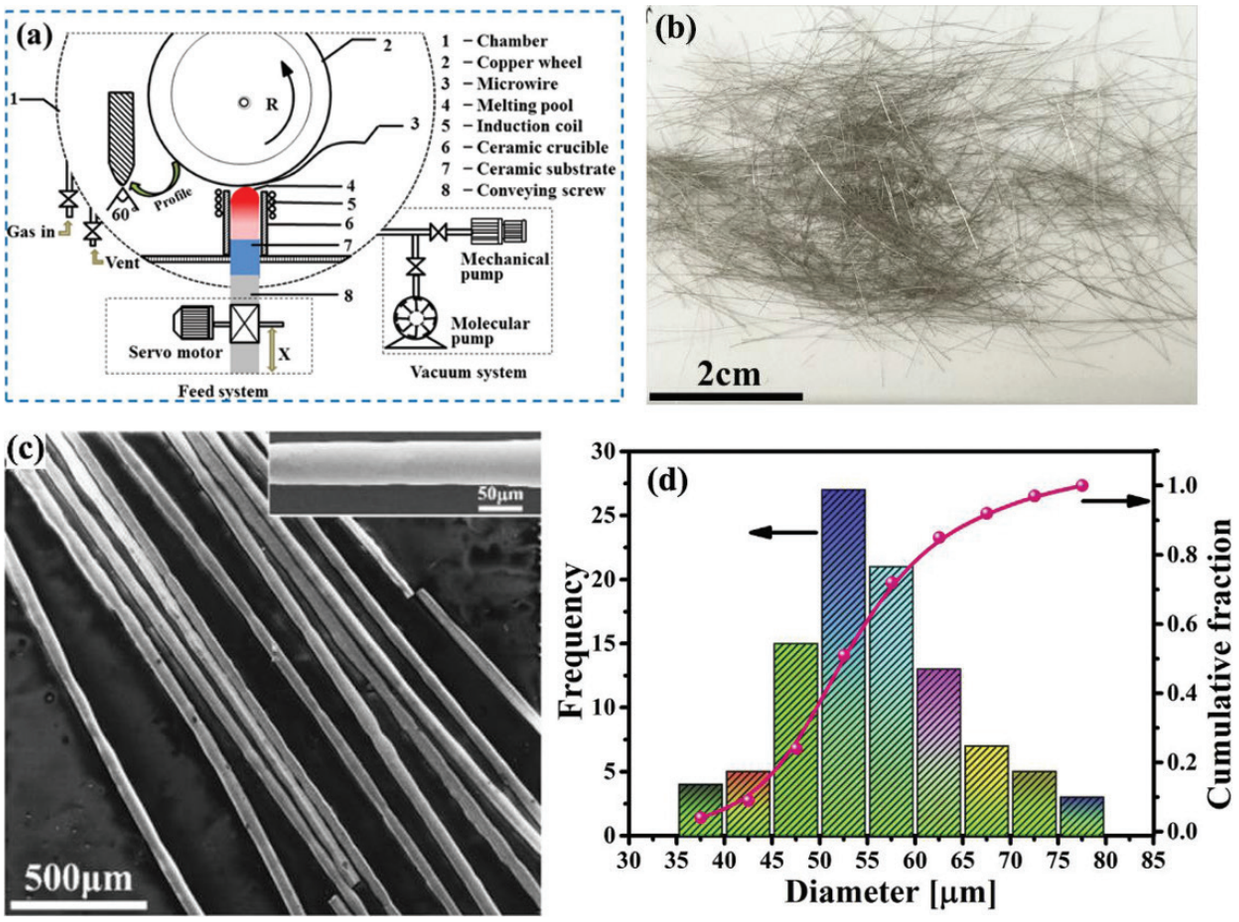

Figure 10. Scheme of the melt extraction process and the obtained Ni-Mn-Ga microwires. (a) Schematic illustration of the melt extraction setup, (b) macroscopic morphology, (c) SEM image, and (d) diameter distribution [13, 18].

crucible and placed into a chamber, (2) the chamber was evacuated to 10^{-3} Pa and then filled with 50 Pa Ar gas, (3) the top part of the ingot was induction heated, thus forming a melting pool in the crucible, (4) the molten phase was driven at a feed rate (V_m) of 40–120 μm/s toward a rotating wheel with wheel rotation velocity (V_w) ranging from 13 to 25 m/s, and (5) the molten alloy was extracted out by the wheel [9]. Typical macroscopic and SEM morphologies of melt-extracted Ni-Mn-Ga microwires are presented in **Figure 10b** and **c**. Microwires with fairly uniform diameter ranging from 45 to 65 μm (**Figure 10d**) were prepared on a large scale with optimized processing parameters: wheel velocity of 23 m/s, feed rate of 60–90 μm/s, and heating power of 20 kW [13].

The microstructural evolution during the melt extraction process, that is, the nucleation behavior of the molten alloy, the unique grain growth behavior, the grain distribution, and the texture, has been systematically studied [13]. As shown in **Figure 11**, microwires with singular nucleation (earlier stage) and dual nucleation (later stage) sites were found at different stages of the preparation: at the beginning of the melt extraction process, the wheel tip temperature is low, and crystallization of the molten alloy nucleates at the wheel tip. Subsequently, the molten alloy nucleates at the two sides of the wheel tip when the wheel tip temperature increased.

Unique grain growth behavior was observed along the radial direction, creating columnar grains growing along the crystal <0 0 1> direction with a fanlike texture in the cross section of the microwire, as shown in **Figure 11**. Finally, at the later stage of the crystallization, the texture evolved into <0 0 1> crystal orientation perpendicular to the flattened surface of the microwire, as shown in **Figure 12**. On this occasion, assuming 5M martensite was formed in the microwires, only variants with *a*-axis [1 0 0] or *c*-axis [0 0 1] perpendicular to the flattened part could exist. The reduced number of twin variants may reduce the incompatibility and thus favor the MFIS.

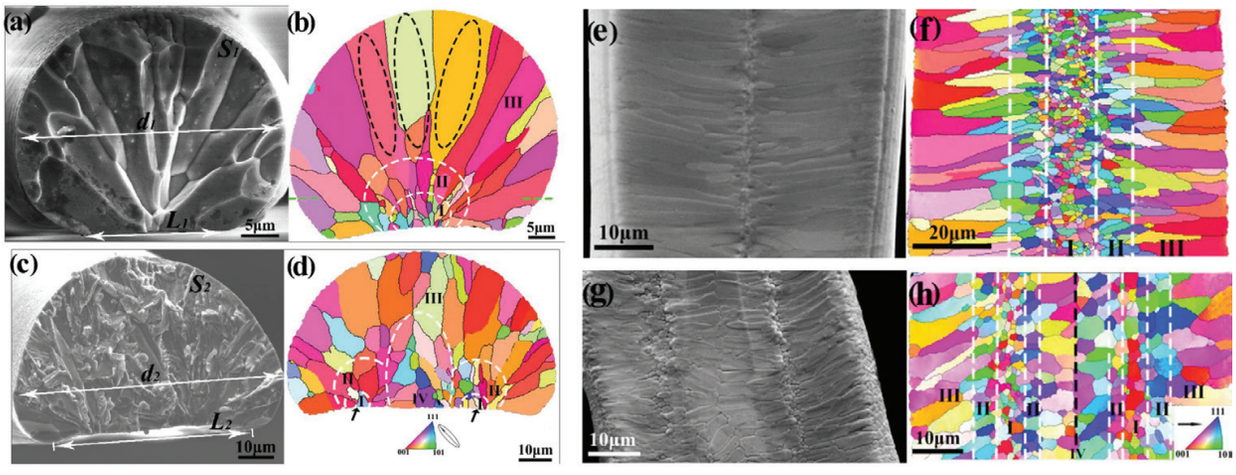

Figure 11. SEM images (a, c, e, g) and EBSD orientation maps (b, d, f, h) of the cross section (a–d) and the longitudinal section (e–h) of the melt-extracted Ni-Mn-Ga microwires [13].

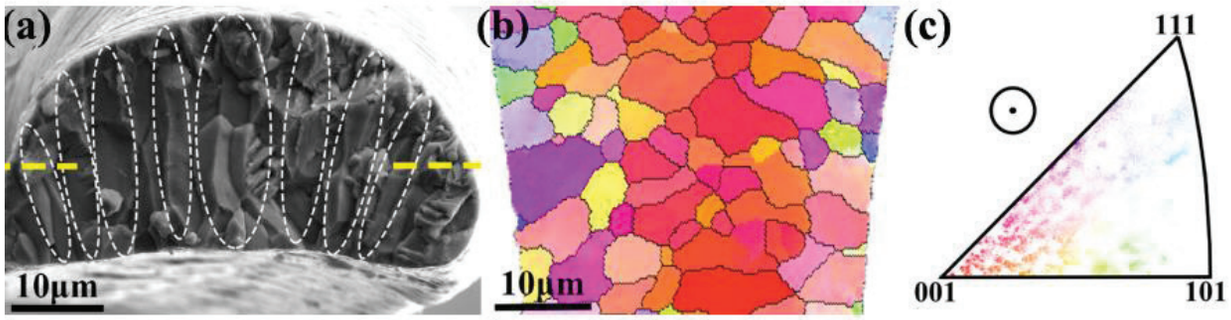

Figure 12. (a) SEM image, (b) EBSD orientation map, and (c) discrete inverse pole figure with respect to (b) of the melt-extracted Ni-Mn-Ga microwires at later stage [13].

4. Martensite transformation of ferromagnetic shape memory alloys

4.1. First-order martensite transformation

4.1.1. Conventional martensite trasnformation

Upon cooling, like in steel, ferromagnetic shape memory alloy undergoes a diffusionless phase transformation from the austenite state to the martensite state, named martensite transformation (MT). Owing to the diffusionless character of the transformation, a slight change of the position of the atoms in cubic austenite phase during cooling leads to a tetragonal distortion of the unit cell.

As was mentioned in Section 2.2, Heusler alloys possess two important phases: the cubic austenite phase and the martensite phase (with different lattice structures). The MT process can be illustrated based on **Figure 13** [17]: upon cooling from an austenite state, the sample starts to form martensite at the martensite start temperature, M_s. The sample is fully transformed to martensite state below the martensite finish temperature, M_f. During the reverse transformation when the sample heats from a fully martensite state, the austenite starts to form above the austenite start temperature, A_s, and is completely transformed to austenite above the austenite finish temperature, A_f.

As shown in the DSC curve of **Figure 13** (upper), the transition from the austenite to martensite is an exothermic reaction, which means that heat is released for this process and the enthalpy change of the system is negative. On the other hand, the reverse transformation from martensite to austenite is an endothermic reaction with a positive enthalpy change. Besides, during DSC measurements, the temperatures at maximum endothermic and exothermic heat flow are defined as A_p and M_p, respectively. While as shown in the magnetization-temperature (M-T) curves of **Figure 13** (lower), the A_p and M_p are derived from the peak values of the first derivative plot of the curves during heating and cooling, respectively (shown in the inset). Martensite transformation is a first-order phase transformation (FOT). A FOT is usually accompanied by an inevitable transformation hysteresis, which can be interpreted by $|A_p - M_p|$ or $(A_s - M_s + A_f - M_f)/2$.

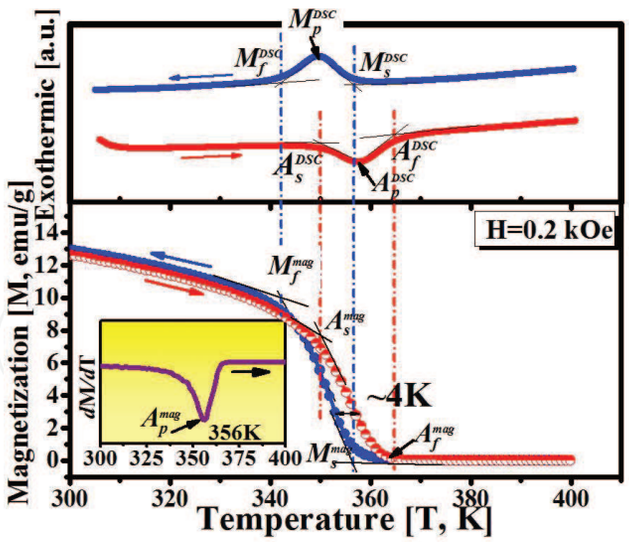

Figure 13. Heating and cooling of DSC curves (upper) and *M-T* curves at low magnetic field of ferromagnetic shape memory alloys [17].

The MT temperatures are very sensitive to the composition for the alloys. For Ni-Mn-Ga and other Ni-Mn-X alloys, the composition dependence of the MT temperatures has been demonstrated in Section 2.1 of the present chapter.

4.1.2. Premartensite transformation

Premartensite transformation (PMT), a weak FOT of the austenite into a micromodulated premartensite phase prior to the martensite transformation itself, has been observed in Ni-Mn-Ga alloys with T_c well above the MT temperature, that is, mainly in Ni-Mn-Ga alloys from Group I (**Table 1**) with near-stoichiometric composition [31, 42]. A PMT at ~260 K has been found in Ni_2MnGa alloys prior to its MT [43], with the austenite phase transformed to an orthogonal three-layer modulated structure, which is similar as the 5M and 7M modulated structure [44].

Existence of unusual physical property change has been found around the PMT temperature during cooling. Firstly, before the PMT, the samples started to exhibit a drastic increase of elastic modulus [32]. Furthermore, the internal friction is increasing from zero to a maximum in the premartensite phase and decreases again in martensite [31]. This sudden soft mode phonon freezing can only be observed in the premartensite phase before the MT; thus, this transformation is defined as the PMT.

4.1.3. Intermartensite transformation

Intermartensite transformation (IMT), a structural transformation from one martensite to another, has been found in high-temperature Ni-Mn-Ga alloys, that is, mainly in Ni-Mn-Ga alloys from Group III (**Table 1**). Upon cooling in these samples, the austenite phase changes to a 5M then 7M and then non-modulated phase or to 7M and then non-modulated phase or directly from austenite to non-modulated phase [32]. While upon heating, only a phase

transformation from the non-modulated martensite to austenite was observed [45]. On the other hand, the IMT can also be induced with increasing stress following the same transformation routes as is induced with decreasing temperature [32].

4.2. Second-order magnetic transformation

The increased distance between the Mn atoms in the Ni-Mn-Ga $L2_1$ structure changes the Mn-Mn exchange interaction from antiferromagnetic of pure Mn to ferromagnetic [33]. Therefore, a magnetic transformation is taking place at the Curie temperature (T_c) from a ferromagnetic phase to a paramagnetic phase upon heating. The magnetic transformation is a second-order transformation (SOT) with no latent heat associated with the phase transformation and can be easily detected from the M-T curves with a drastic falling of the magnetization. The T_c of the Heusler alloys is also influenced by the composition and, thus, can be tuned. In our previous work, the MT temperature was increased, and the T_c was lowered after Cu doping in Ni-Mn-Ga alloy, leading to an overlap of the martensite and magnetic transformation, that is, magneto-structural coupling, in the microwire. The magneto-structural coupling enhanced the MCE of the alloy [17].

5. Properties and application of ferromagnetic shape memory alloys

5.1. Magnetic-field-induced strain (MFIS)

5.1.1. Overview of MFIS

Magnetic-field-induced strain (MFIS) comes from twin boundary motion under the application of a magnetic field, which is driven by the magnetostress produced by high magnetocrystalline anisotropy of the Ni-Mn-Ga alloy and its low twining stress [35], as schematically illustrated in **Figure 14** [46]. The MFIS property is useful for actuation and sensing purposes [47]. MFIS was firstly reported in 1996 by Ullakko et al. [5]. A strain of 0.19% under a magnetic field of 0.43 T was obtained from a Ni_2MnGa sample at 265 K. From then on, the interest of the MFIS in FSMAs grew rapidly all over the world. Besides, many different compositions, such as Ni-Fe-Ga [48], Ni-Mn-In [49], Co-Ni-Al [50], Co [51], Fe [52], and rare earth [53]-doped Ni-Mn-Ga alloys, have also been investigated.

So far, large MFIS (~1–10%) has been achieved only for Ni-Mn-Ga single crystals [6, 7]. The most representative one was reported in 2000, when Murray et al. [6] achieved a 6% MFIS in a 5M single-crystalline Ni-Mn-Ga alloy at room temperature under a magnetic field of 0.62 T. During the experiment, different stresses were applied to restore the MFIS and to measure the magnetostress. After that, in 2002, Sozinov et al. [54] published a giant MFIS of about 9.5% in 7M Ni-Mn-Ga single crystals at ambient temperature in a magnetic field of less than 1 T. However, the fabrication of single crystals is difficult because of sever segregation, low growth speed, and high cost. On the other hand, polycrystalline Ni-Mn-Ga alloys may be produced with much lower cost, but their MFIS is vanishingly small (<0.01%) because of the low mobility of twin boundaries constrained by grain boundaries [55, 56]. Many works have been

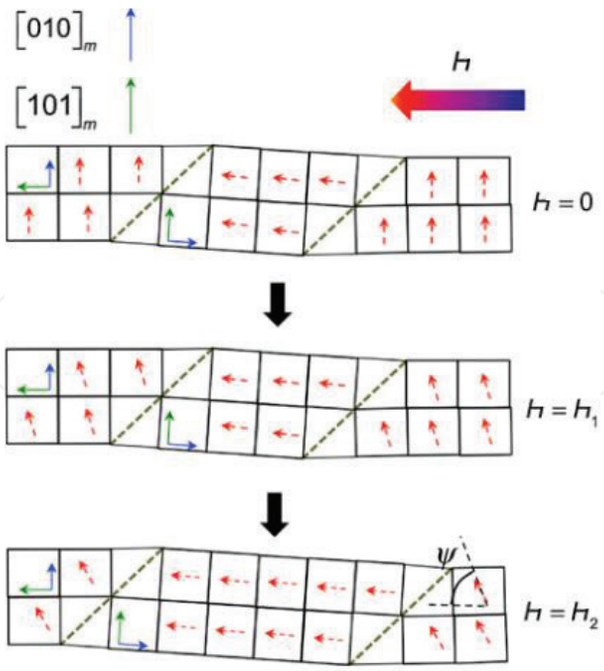

Figure 14. Schematic illustration of rotation of magnetic moments and twin boundary motion in tetragonal FSMAs under magnetic fields [46].

carried out to enhance their MFIS up to 1% by introducing strong textures and subsequent training in coarse-grained polycrystalline Ni-Mn-Ga alloys [57–60]. Recently, considering the hindering effect of the grain boundaries on the twin boundary motion, approaches regarding reduction of grain boundaries, that is, by producing a porous material (foam) or reducing sample size, have been carried out, which will be discussed in detail in Sections 5.1.2 and 5.1.3.

5.1.2. MFIS in Ni-Mn-Ga foams

As mentioned earlier, fine-grained polycrystalline Ni-Mn-Ga alloys are easier to fabricate but with vanishingly small strain due to the constraints provided by the grain boundaries. Introducing porosity in Ni-Mn-Ga alloys not only reduces the constraints imposed by grain boundaries but also maintains the ease of processing associated with casting polycrystalline Ni-Mn-Ga. After certain grain growth heat treatment, the twins can span between the pores, as shown in **Figure 15** [10]. As a result, the twin boundaries can move as freely as in single-crystalline bulk material within the grains.

Research work regarding the MFIS in Ni-Mn-Ga foams was firstly reported by the research group of Müllner et al. [9]. With 76% open porosity, the foam displayed a fully reversible MFIS as large as 0.12% with excellent stability over 25 million magnetomechanical cycles. Thereafter, the same group further increased the MFIS to 2.0–8.7% in dual-pore Ni-Mn-Ga foams (**Figures 7b** and **8b**) with 62% porosity after thermo-magneto-mechanical cycling training [10]. These obtained strains are much larger than those of any polycrystalline and comparable to those of single crystals. Different from bulk single or polycrystalline alloy, these open-porosity foams allow fluid flow, making them potentially useful as micro-pumps and magnetocaloric materials [10].

Figure 15. Optical micrograph of twins in Ni-Mn-Ga foam, extending entirely from pore to pore (black) [10].

5.1.3. MFIS in Ni-Mn-Ga microwires

Constraint of twin boundary caused by grain boundary is three dimensional in bulk alloys and two dimensional in thin films. It can be further reduced to one dimensional in microwires. Furthermore, by reducing sample size, small-sized Ni-Mn-Ga alloys show low inertia [61], low eddy current loss at high frequency [62], high magnetocrystalline anisotropy, and work output [63]. Recently, oligocrystalline microwires with bamboo or near-bamboo structures have attracted much interests owning to a less constrained environment and more free surface [64–66], which makes them the closest approximation to single crystals. The micrographs of Ni-Mn-Ga and Cu-Al-Ni oligocrystalline microwires are presented in **Figures 16** and **17**, respectively. Martensite plates spanning across the wire diameter can be observed [65, 66].

However, because of the lack of textures, only a subset of grains was prone to favorably oriented to show a detectable MFIS. Approximately 1% MFIS was found in a not-constrained and randomly textured Ni-Mn-Ga without bias stress by magnetizing the microwire parallel and perpendicular to the wire axis up to 2 T [11]. Recently, a 1 T rotating magnetic field caused the Ni-Mn-Ga microwire to bend to a curvature corresponding to a surface strain of 1.5% [40]. Mechanical or the combined thermo-magneto-mechanical training in martensite state may effectively lower the twining stress, to form preferential oriented variants [9, 58], and, thus, may in favor of achieving a high MFIS in oligocrystalline microwires. The realization of large MFIS in one-dimensional microwires may provide a wide prospect in the application of micro-actuators and sensors.

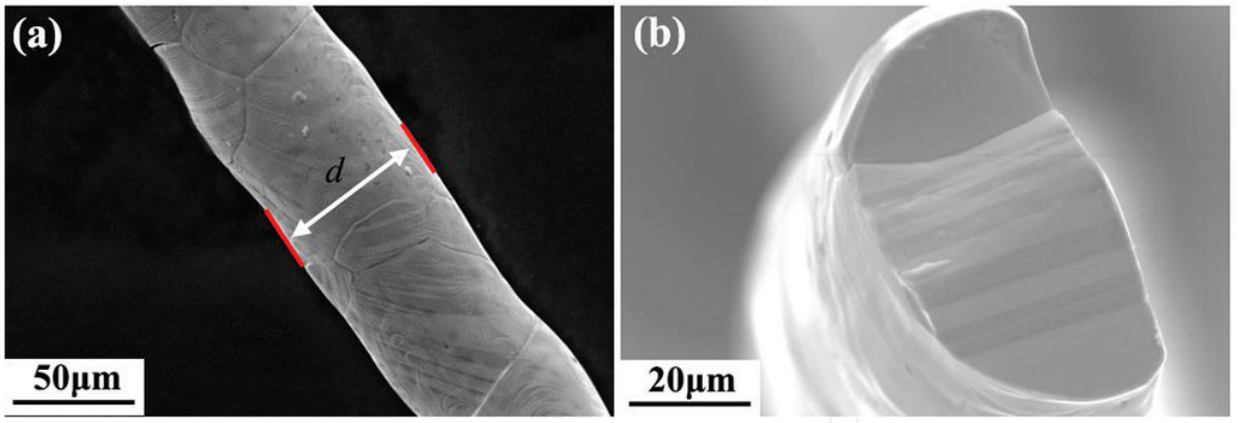

Figure 16. SEM micrographs of (a) free surface and (b) cross section of Ni-Mn-Ga oligocrystalline microwires prepared by melt extraction and subsequent heat treatment [66].

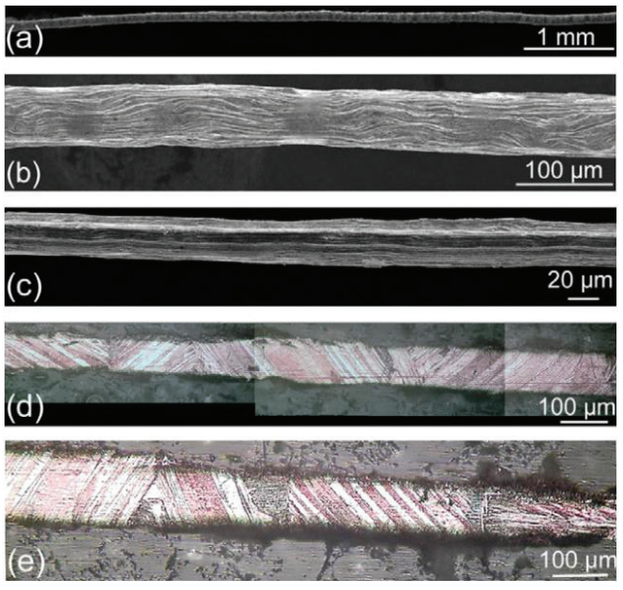

Figure 17. (a–c) Micrographs of Cu-Al-Ni oligocrystalline microwires prepared by Taylor method and subsequent heat treatment. (d and e) Montaged optical micrographs of the longitudinal section of the wire [65].

5.2. Magnetocaloric effect (MCE)

5.2.1. Overview of MCE

Magnetic refrigeration, based on the magnetocaloric effect (MCE), has attracted interests as a potential alternative to well-established compression-evaporation technique for room temperature refrigeration because of the compactness, high efficiency, and environmental friendship. To characterize a MCE, the adiabatic temperature change (ΔT_{ad}), the magnetic entropy change (ΔS_M), and the relative cooling power (*RCP*) should be measured. The most recently researched ambient magnetic refrigeration materials (MCM) mainly include $La(Fe,Si)_{13}$ based [67–70] and $Gd_5(Si,Ge)_4$ based [67, 71] alloys (contain rare-earth elements) and MnAs based [67, 72–74],

MnFe(P,X) (X = As, Ge, Si) [75, 76], Fe-Rh [77], NiMn based [78–82] alloys (rare-earth free). These types of materials undergo a first-order magnetic phase transition (FOMT), exhibit large hystereses, and show a large value of ΔS_M. For example, with a magnetic field change $\Delta H = 5$ T, $\Delta S_M = 35–50$ J/kg K for MnAs-based [73], $Gd_5(Si,Ge)_4$-based [67], and $La(Fe,Si)_{13}$-based [83] alloys and $\Delta S_M = 35–40$ J/kg K for Ni-Mn-In-Co [84] and Ni-Mn-Sn [85] alloys were obtained. For some MCE, the low working temperature span (ΔT_{FWHM}) and high thermal and magnetic hysteresis loss [86, 87] limit their applications. MCM with reduced dimensions (particle, microwire, film, or foam) [88, 89] have been proposed to broaden the ΔT_{FWHM} by preparing the alloy with gradient composition distribution state. In addition, deduction in dimensions is an effect way to decrease the hysteresis loss by reducing internal stress and the constraints between grains attributed to the high surface-area-to-volume ratio [19].

5.2.2. MCE in Ni-Mn-based alloys

Very recently, we reported magnetocaloric effects of high-content Fe-doped $Ni_{44.9}Fe_{4.3}Mn_{38.3}Sn_{12.5}$ polycrystalline microwires prepared by a melt extraction technique [18], as displayed in **Figure 18**. Under a magnetic field of 20 kOe, the ΔS_m peak value, related to the first-order martensite transformation (FOMT) of the present $Ni_{44.9}Fe_{4.3}Mn_{38.3}Sn_{12.5}$ microwires, reaches 3.0 J/kg K, which is comparable to the $Ni_{44}Fe_6Mn_{40}Sn_{10}$ ribbons (1.8 J/kg K under 20 kOe) [90] and $Ni_{51.6}Mn_{32.9}Sn_{15.5}$ films (1.5 J/kg K under 10 kOe) [91]. The second-order martensite transformation (SOMT) related to ΔS_m of −3.7 J/kg K and ΔT_{FWHM} of ~85 K under 5 T is comparable to that of $Ni_{48.8}Mn_{26.7}Ga_{20.8}Cu_{3.7}$ microwires (−8.3 J/kg K with ΔT_{FWHM} of 13 K under 5 T) [19] and $Ni_{53.5}Mn_{23.8}Ga_{22.7}$ films (−8.5 J/kg K with ΔT_{FWHM} of 17 K under 6 T) [92]. The studied $Ni_{44.9}Fe_{4.3}Mn_{38.3}Sn_{12.5}$ microwires, exhibiting large surface-area-to-volume ratio, giant MCE property, and low cost, may act as potential magnetic refrigerants.

As shown in **Figure 19a**, the ΔS_m of $Ni_{48}Mn_{26}Ga_{19.5}Fe_{6.5}$ microwires [19] with a diameter of ~50 μm shifted from positive to negative to the applied field is higher than 0.5 T. These interesting positive-to-negative ΔS_m transition behaviors have also been found in $Ni_{50.1}Mn_{20.7}Ga_{29.6}$ single crystal at 0.8 T [93] and $Ni_{54.5}Fe_1Mn_{20}Ga_{24.5}$ polycrystalline alloy at 0.5 T [94]. The maximum negative ΔS_m is ~4.7 J/kg K under 5 T corresponding to magnetic-field-induced structural transition from martensite to austenite phase. At 20 kOe, ΔS_m in the microwires is 1.71 J/kg K, which is comparable to Ni-Fe-Mn-Ga alloy (2.1 J/kg K) [94]. Moreover, the value of ΔS_m observed at magnetic transition under 3 T is 2.05 J/kg K in Fe-doped $Ni_{54.5}Fe_1Mn_{20}Ga_{24.5}$ microwires. Compared to the un-doped $Ni_{50.95}Mn_{25.45}Ga_{23.6}$ microwires, the ΔS_m is about three times higher under the same magnetic field [95].

It can be seen from **Figure 19b** that the annealed $Ni_{48.8}Mn_{26.7}Ga_{20.8}Cu_{3.7}$ microwires [87] exhibited magneto-structural coupling and wide martensitic transformation temperature range, which contribute to a ΔS_m of 8.3 J/kg K with a wide ΔT_{FWHM} of 13 K under a magnetic field of 5 T. The obtained RC in Ni-Mn-Ga-Cu microwire (78.0 J/kg) is comparable with those of Ni-Mn-based alloys (70–115 J/kg) [96] and superior to those of Ni-Mn-Ga-Cu bulk alloys (72–75 J/kg) [97–99]. On the other hand, when compared to Gd [100] or $LaFe_{13-x}Si_x$ [101] alloys, the Ni-Mn-Ga-Cu microwires are rare-earth free and thus cost-effective, which helps for the practical applications.

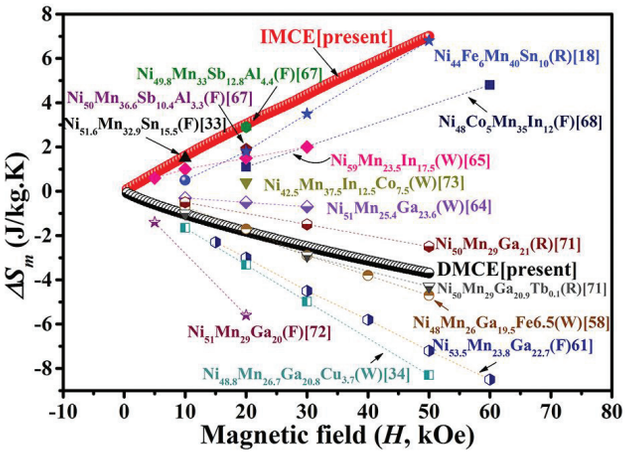

Figure 18. The ΔS_m as a function of external magnetic field in the present $Ni_{44.9}Fe_{4.3}Mn_{38.3}Sn_{12.5}$ microwires and some other Ni-Mn-Z-based (Z = Sn, Sb, In, Ga) Heusler compounds in the forms of ribbons (R), thin films (F), and microwires (W) [18].

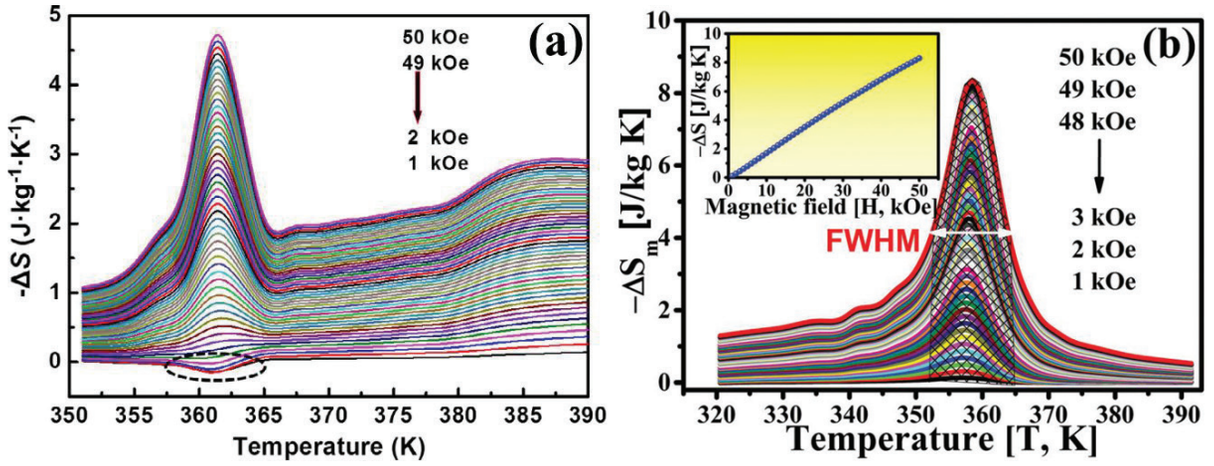

Figure 19. Entropy changes as a function of temperature for (a) $Ni_{48}Mn_{26}Ga_{19.5}Fe_{6.5}$ [19] and (b) $Ni_{48.8}Mn_{26.7}Ga_{20.8}Cu_{3.7}$ [17] microwires under different magnetic fields.

5.3. Shape memory and superelasticity

In Sections 5.1 and 5.2, Ni-Mn-Ga alloy has been demonstrated to exhibit high MFIS and excellent MCE properties both driven by external magnetic field. Actually, due to the thermoelastic MT, Ni-Mn-Ga alloys also show well-pronounced thermal field-induced superelasticity (SE, stress-induced MT at austenite state and recovered upon unloading) [45], one-way shape memory effect (OWSME, deformed under stress at martensitic state and recovered during heating), and two-way shape memory effect (TWSME, shape change between martensite and austenite states continuously upon heating and cooling) [8, 9], which is similar to traditional SMAs, such as Ni-Ti.

So far, OWSME strain up to ~6.1% [102] and SE ~6% [45] has been achieved in Ni-Mn-Ga single crystals under compression mode. TWSME induced by training has reached 9% in

single-crystalline Ni-Mn-Ga alloy [8] under tension mode. On the other hand, related reports for SME and SE properties for bulk polycrystalline Ni-Mn-Ga alloys are relatively seldom and lower than those of single crystals [102, 103]. Besides, due to the intrinsic brittleness of the alloy, previous reports are mostly focused on the compression processes than on the tension mode.

5.3.1. Shape memory effect and superelasticity in Ni-Mn-Ga microwires

Due to the transcrystalline fracture tendency of polycrystalline Ni-Mn-Ga alloys, efforts have been made to enhance their ductility. Microstructure refinement and sample size reduction have been proven to lower the brittleness [6, 9]. Recently, small-sized Ni-Mn-Ga microwires have been made by rapid solidification methods involving Taylor method and melt extraction technique to investigate the SME and SE properties [12, 14, 39, 40]. A large reversible SE strain of 10.9% has been reported in polycrystalline Ni-Mn-Ga glass-coated wires tested in tension mode [39]. The Taylor method as applied to Ni-Mn-Ga microwire fabrication allows production of wires with a uniform circular cross section while with lower efficiency compared with the melt extraction technique. In this section, the SME and SE in melt-extracted microwires are displayed based on our previous work.

Ni-Mn-Ga microwires prepared by melt extraction technique exhibited a higher reversible SE strain and recoverable SME strain compared with bulk parent alloys [12]. **Figure 20** displays the typical recoverable SME curve of as-extracted Ni-Mn-Ga microwire, and A–C demonstrates the SME strain regarding twin boundary motion after unloading (~1.5%). Unlike single crystals, the twin boundary motion process did not show a stress plateau upon loading (A–B) due to the refinement of the grains.

Owing to the rapid solidification process during fabrication, high internal stresses, reduced degree of atomic order, and other defects may affect the SME and SE properties in the as-extracted microwires. A stepwise chemical ordering annealing was carried out, and the effect of annealing on the SE behavior was investigated in our previous work [14]. SE comparison before and after annealing is shown in **Figure 21**. Annealing decreases the stress-induced MT (SIM) stress and the hysteresis and improves the reversibility during superelastic cycling.

Furthermore, polycrystalline Ni-Mn-Ga microwires exhibit higher-temperature dependences compared with Ni-Mn-Ga single crystals and conventional superelastic alloys (**Figure 22**), which are considered to be related to the small grains achieved by melt extraction. Besides, the temperature dependences of the microwires are lowered after annealing (inset II), that is, the slope ($d\sigma_{As}/dT$) of the annealed microwire, 15.6 MPa/K, is smaller than that of as-extracted one, 17.5 MPa/K, revealing an easier reverse transformation process in the annealed microwire.

Above all, melt-extracted Ni-Mn-Ga microwires after annealing exhibit lower SE stresses, lower-temperature dependences, and higher SE reversibility. Besides, the preparation is convenient and efficient. Given these properties, Ni-Mn-Ga microwire is expected to be used for practical applications, such as superelastic materials, micro-actuator materials, and microsensor materials in various fields.

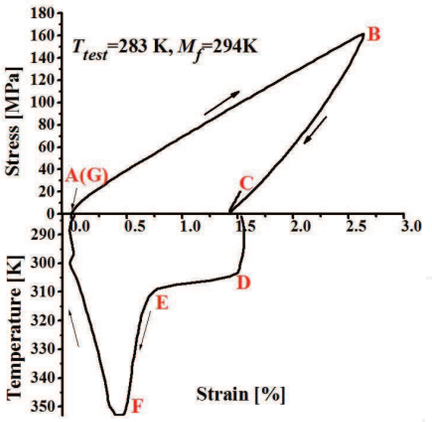

Figure 20. Tensile stress-strain curves of as-extracted Ni-Mn-Ga microwires at martensite state.

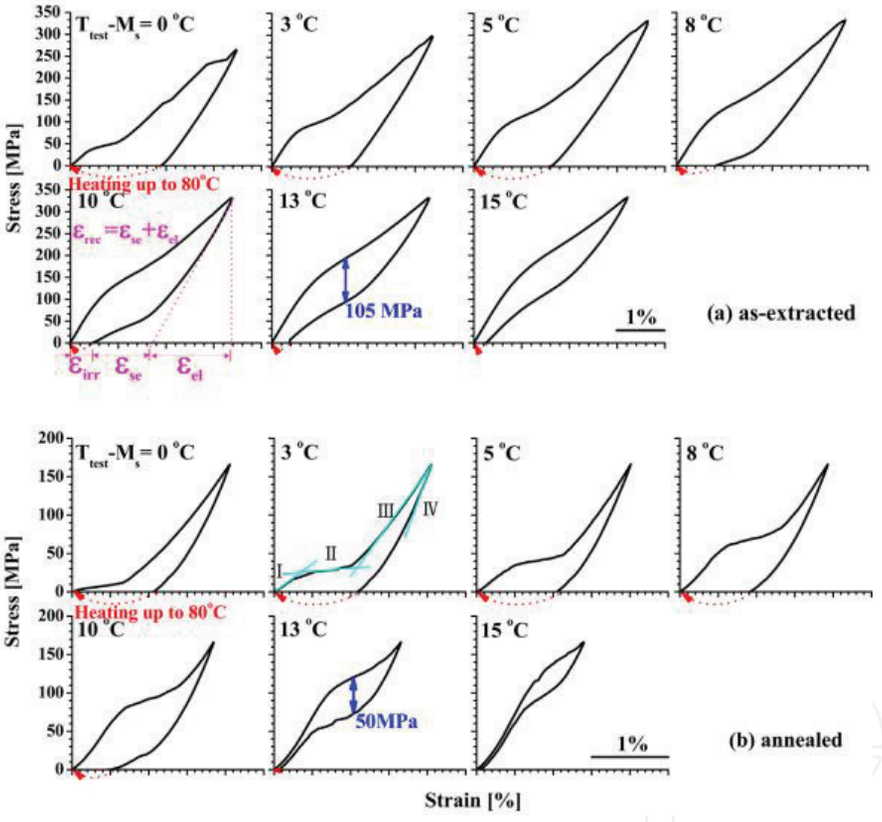

Figure 21. Tensile stress-strain curves of (a) as-extracted and (b) annealed Ni-Mn-Ga microwires at temperature levels (T_{test} – M_s) approximately from 0 to 15°C at austenite state (equilibrate at 80°C and then cool down to T_{test}). ε_{irr}, ε_{se}, and ε_{el} stand for the irreversible strain (recovered upon heating), strain recovery upon reverse transformation, and elastic recovery, respectively [14].

5.3.2. Shape memory effect and superelasticity in Ni-Mn-Ga-Fe microwires

The ductility of Ni-Mn-Ga alloys can be enhanced by the fourth element doping [104–106]. Among various doping elements, Fe has attracted many attentions [107, 108]. In our previous work, SME and SE behaviors of $Ni_{50}Mn_{25}Ga_{25-x}Fe_x$ (x = 1–6%) microwires (diameter ~30–40 μm)

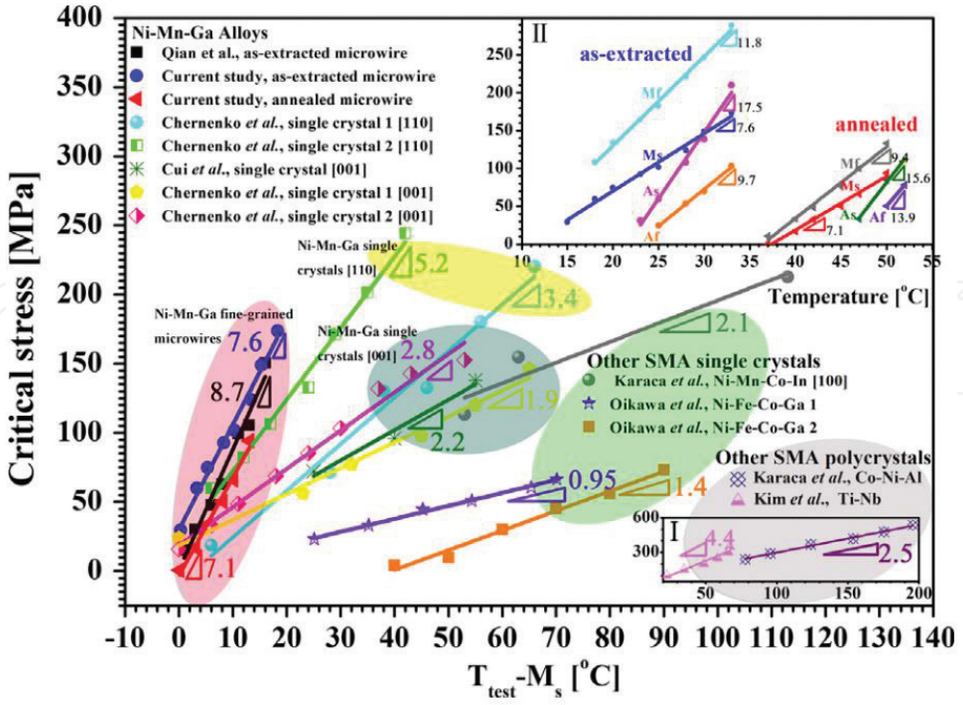

Figure 22. SIM critical stress (σ_{Ms}) vs. temperature plots of the Ni-Mn-Ga microwires and other alloys [14].

were investigated [16]. OWSME and TWSME curves of the $Ni_{49.7}Mn_{25}Ga_{19.8}Fe_{5.5}$ microwires are shown in **Figure 23a** and **b**, respectively. An OWSME strain of ~1.0% was induced by stress at its martensite state under tension mode in the microwire and completely recovered upon heating to its austenite state (**Figure 23a**). With respect to the TWSME, the application in sensors is generally used under certain applied stress in thermal cycle. Different external stresses were applied during the thermal cycling; fully recoverable strain was obtained in the

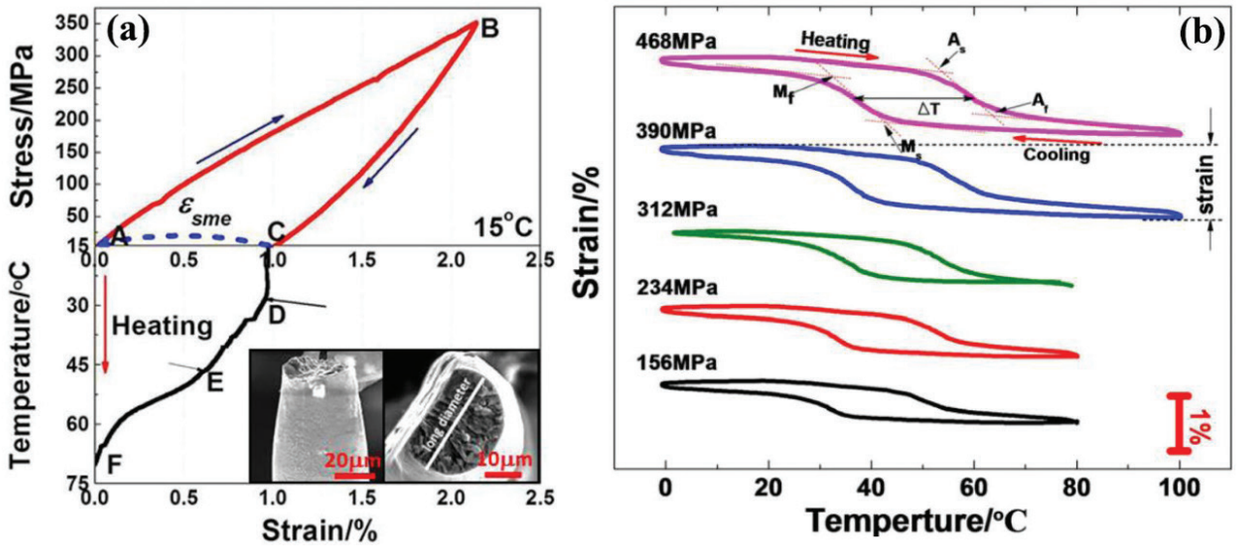

Figure 23. Tensile stress-strain curves of $Ni_{49.7}Mn_{25}Ga_{19.8}Fe_{5.5}$ microwires. (a) OWSME and (b) TWSME [16].

$Ni_{49.7}Mn_{25}Ga_{19.8}Fe_{5.5}$ microwire (**Figure 23b**). The TWSME strain of the microwire increased from 0.84% at 156 MPa to 1.504% at 468 MPa.

The SE behavior of the $Ni_{50}Mn_{25}Ga_{25-x}Fe_x$ (x = 4.5) was studied due to its favorable MT temperature near RT. The SE tensile stress-strain curves obtained at various temperatures in $Ni_{50}Mn_{25}Ga_{25-x}Fe_x$ (x = 4.5) are demonstrated in **Figure 24**.

The SE of $Ni_{50}Mn_{25}Ga_{25-x}Fe_x$ (x = 4.5) microwires shows similar behavior as that of Ni-Mn-Ga microwires [9]. The maximum strain recovery rates achieved in $Ni_{50}Mn_{25}Ga_{25-x}Fe_x$ (x = 4.5) are 94 and 90%, respectively, which was higher than that in as-extracted Ni-Mn-Ga microwires while lower than Ni-Mn-Ga microwires after chemical ordering annealing.

5.4. Application of ferromagnetic shape memory alloys

Ni-Mn-Ga alloys may act as actuator by making the use of the large MFIS and magnetic shape memory effect (MSM) or as sensor related to the dependence of the magnetization change under an external compressive stress. For MFIS/MSM, the working frequency is high because they are driven by external magnetic fields. This character is superior to the traditional shape memory alloys, such as Ni-Ti, which are driven by temperature change and thus only work at much smaller frequency. Some typical examples of the actuators created based on the ferromagnetic shape memory alloys are shown in **Figures 25–27**.

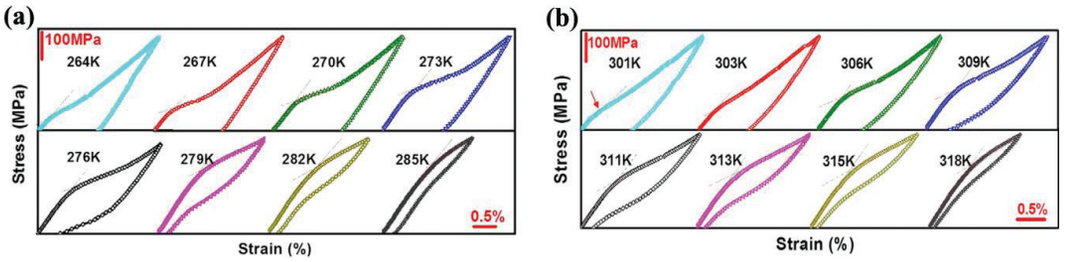

Figure 24. Tensile stress-strain curves obtained at various temperatures in $Ni_{50}Mn_{25}Ga_{25-x}Fe_x$ microwires. (a) x = 4 and (b) x = 5 [15].

Figure 25. MSM-spring actuator (MAGNETOSHAPE® by ETO MAGNETIC GmbH) [109].

Figure 25 demonstrates the most straightforward MSM-spring actuator: the elongation is obtained by a magnetic field perpendicular to the motion, while contraction is obtained thanks to the elastic force of a spring. The magnetic field induces a magnetostress in the MSM alloy. In the spring actuator, such a magnetic force must work always against the elastic force of the spring, which is bigger at bigger strain [109].

Figure 26a presents another important MSM actuator: push-push or multistable actuator [109]. It is composed of two MSM units which arranged antagonistically. In this case, one element acts as a load for another one. The movement in both directions can be controlled magnetically. There is the moving rod in yellow on the top. **Figure 26b** shows an application of a push-push actuator: the MSM device is used to move a mirror on the top and redirect an optical signal.

For FSMA thin films, a novel actuation mechanism has been developed, which makes use of both the ferromagnetic transition and the martensitic transformation. The mechanism is illustrated in **Figure 27** for a Ni-Mn-Ga bending actuator placed in the inhomogeneous magnetic field of a miniature permanent magnet.

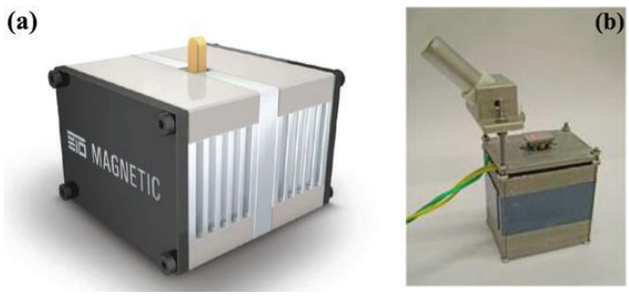

Figure 26. (a) Example of MSM push-push actuator (MAGNETOSHAPE® by ETO MAGNETIC GmbH). (b) Optical switch actuated by a push-push actuator (Lappeenranta University of Technology, Finland) [109].

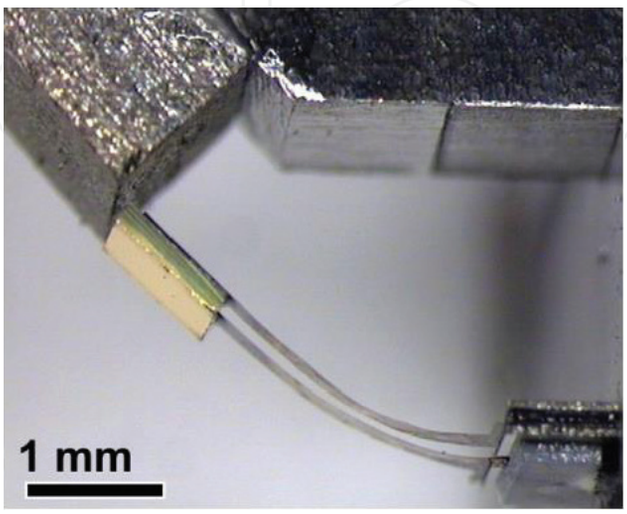

Figure 27. Prototype of a FSMA micro-actuator for control of a micro-mirror [110].

Depending on the temperature of the micro-actuator, either magnetic or shape recovery forces occur in opposite directions, while the corresponding biasing forces remain small. Thus, an almost perfect antagonism can be realized in a single component part. By applying an alternating electrical current, a periodic oscillation of the beam can be excited. This motion can be used to control the deflection of a micro-mirror attached to the front end of the actuator. For instance, a micro-scanner prototype has been developed based on the actuation mechanism (see **Figure 27**). The overall dimensions are 7 mm × 2 mm × 5 mm.

The micro-pump shown in **Figure 28**, developed in Peter Müllner's lab at Boise State University, may deliver sub-microliter volumes of dugs directly to specific regions of the brain. The micro-pump was small and robust and can be placed on a head stage on a rat so that drugs can be delivered and brain activity can be monitored while the rat is moving about [111].

Figure 29 shows a prototype of an energy harvester realized by former Adaptamat [109]. A repeated application of tension and compression force deforms the MSM material and induces a voltage in the coil. Such a voltage can be used to supply energy to a small load. Theoretically, the maximum energy per volume unit that can be extracted from an MSM alloy is equal to the work output, that is, about 150 kJ/m^3.

In Ni-Mn-Ga alloys, the first-order martensite transformation (FOMT) and second-order magnetic transition (SOMT) produce traditional MCE [112], as displayed in **Figure 30a**. On the other hand, in Ni-Mn-Z-based (Z = Sn, In, Sb) alloys, both direct and inverse MCE (see **Figure 30b**) may be created. The inverse MCE originates from a metamagnetic structural

Figure 28. Micro-pump created based on Ni-Mn-Ga alloys [111].

Figure 29. Energy harvester based on MSM alloys developed by Adaptamat [109].

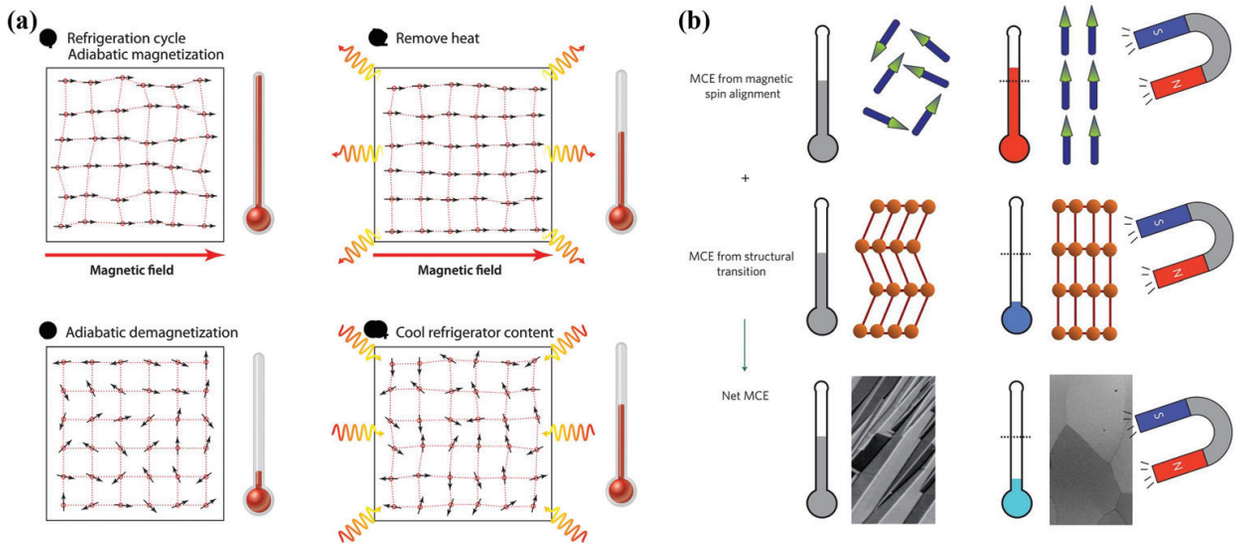

Figure 30. Schematic illustration of (a) traditional magnetocaloric effect [112] and (b) inverse magnetocaloric effect [21].

transition from the paramagnetic/antiferromagnetic martensite to ferromagnetic austenite under a bias magnetic field [21], while the direct MCE is attributed to the magnetic transition of the austenite phase around its Curie point [113]. The first-order martensite transformation (FOMT) is responsible for such inverse MCE, which usually exhibits a huge ΔS_m and a large adiabatic temperature change ΔT_{ad} but rather low ΔT_{FWHM} and high hysteresis loss [86]. Ni-Mn-In-Co alloys may also produce giant stress output through magnetic-field-induced martensite transformation [20].

6. Conclusions remarks

The martensite transformation temperature of FSMAs is sensitive to the composition, while the magnetic transition temperature is less sensitive to the composition. Some empirical formula has been summarized to build the relationship between the transformation temperatures and compositions. In addition, the martensite and austenite crystal structures as well as the magnetic properties of these alloys have been extensively investigated.

Single-crystalline FSMAs, such as Ni-Mn-Ga alloys, have been widely studied because the high MFIS is usually generated in the single-crystalline alloys since low resistant to the twin boundary motion. The compositional segregation during the growth of single-crystalline alloys has to be carefully controlled in order to fabricate the alloy ingots with repeatable MFIS. On the other hand, polycrystalline alloys may be fabricated by low-cost methods, such as casting. The polycrystalline Ni-Mn-Ga foams produced by replication casting may generate MFIS as high as 8.7% after suitable training.

Polycrystalline microwire may be synthesized on a large scale by melt extraction, which exhibits pronounced properties, such as MFIS, magnetic entropy change, and superelasticity. Small-sized materials, such as powders, microwires, ribbons, and films, exhibit giant-specific surface area, that is, surface-area-to-volume ratio, which is responsible for the reduced con-

straints to the twin boundary motion, enhanced heat exchange efficiency, and improved magnetic refrigeration hysteresis loss. The underlying mechanisms between the material size and MCE properties need to be further studied.

The martensite transformation in FSMAs may be induced by external heat change, similar to conventional shape memory alloys, such as Ni-Ti, as well as by external magnetic field. As the operation frequency of an external magnetic field can be much higher than a heat field, FSMAs can work at much higher frequencies than conventional Ni-Ti alloys. The high MFIS produced in single-crystalline Ni-Mn-Ga bulk alloys and polycrystalline foams may find application in high-efficient actuators. On the other hand, the magnetization property change of a FSMA occurs under an external mechanical straining, such as compression. By measuring the magnetization or the induction voltage, the FSMAs may act as sensors, such as force, position, or acceleration sensors.

FSMAs attract much attention in the recent years as high-efficient magnetic refrigeration materials. Significant conventional or inverse magnetocaloric effects have been investigated during the martensite and magnetic transformations. For the alloys (i.e., Ni-Mn-Ga alloys) in which the martensite and magnetic transformations produce the same sign of the magnetic entropy change, the creation of the partial and full magneto-structural coupling states by compositional tuning may be adopted to optimize the magnetic entropy change and working temperature interval.

Author details

Xuexi Zhang* and Mingfang Qian

*Address all correspondence to: xxzhang@hit.edu.cn

School of Materials Science and Engineering, Harbin Institute of Technology, Harbin, China

References

[1] Chernenko VA, Vitenko IN. Structural characterization and properties of the Ni_2MnGa ribbon transforming martensitically. Materials Science Forum. 1994;**166-169**:439

[2] Kokorin VV, Chernenko VA, Valkov VI, Konoplyuk SM, Khapalyuk EA. Magnetic transformation in Ni_2MnGa compounds. Fizika Tverdogo Tela. 1995;**37**:3718

[3] Martynov VV. X-ray diffraction study of thermally and stress-induced phase transformations in single crystalline Ni-Mn-Ga alloys. Journal de Physique IV. **1995**;5:91

[4] Chernenko VA, Cesari E, Kokorin VV, Vitenko IN. The development of new ferromagnetic shape-memory alloys in Ni-Mn-Ga system. Scripta Metallurgica et Materialia. 1995;**33**:1239

[5] Ullakko K, Huang JK, Kantner C, OHandley RC, Kokorin VV. Large magnetic-field-induced strains in Ni_2MnGa single crystals. Applied Physics Letters. 1996;**69**:1966

[6] Murray SJ, Marioni M, Allen SM, O'Handley RC, Lograsso TA. 6% magnetic-field-induced strain by twin-boundary motion in ferromagnetic Ni-Mn-Ga. Applied Physics Letters. 2000;**77**:886

[7] Sozinov A, Likhachev AA, Lanska N, Ullakko K, Lindroos VK. 10% magnetic-field-induced strain in Ni-Mn-Ga seven-layered martensite. Journal de Physique IV. 2003; **112**:955

[8] Sozinov A, Lanska N, Soroka A, Zou W. 12% magnetic field-induced strain in Ni-Mn-Ga-based non-modulated martensite. Applied Physics Letters. 2013;**102**:219022

[9] Boonyongmaneerat Y, Chmielus M, Dunand DC, Müllner P. Increasing magnetoplasticity in polycrystalline Ni-Mn-Ga by reducing internal constraints through porosity. Physical Review Letters. 2007;**99**:247201

[10] Chmielus M, Zhang XX, Witherspoon C, Dunand DC, Müllner P. Giant magnetic-field-induced strains in polycrystalline Ni-Mn-Ga foams. Nature Materials. 2009;**8**:863

[11] Scheerbaum N, Heczko O, Liu J, Hinz D, Schultz L, Gutfleisch O. Magnetic field-induced twin boundary motion in polycrystalline Ni-Mn-Ga fibres. New Journal of Physics. 2008;**10**:73002

[12] Qian MF, Zhang XX, Witherspoon C, Sun JF, Müllner P. Superelasticity and shape memory effects in polycrystalline Ni-Mn-Ga microwires. Journal of Alloys and Compounds. 2013;**577**:S296

[13] Qian MF, Zhang XX, Wei LS, Martin PG, Sun JF, Geng L, Scott TB, Panina LV, Peng HX. Microstructural evolution of Ni-Mn-Ga microwires during the melt-extraction process. Journal of Alloys and Compounds. 2016;**660**:244

[14] Qian MF, Zhang XX, Wei LS, Geng L, Peng HX. Effect of chemical ordering annealing on martensitic transformation and superelasticity in polycrystalline Ni-Mn-Ga microwires. Journal of Alloys and Compounds. 2015;**645**:335

[15] Liu Y, Zhang X, Xing D, Shen H, Qian M, Liu J, Chen D, Sun J. Martensite transformation and superelasticity in polycrystalline Ni-Mn-Ga-Fe microwires prepared by melt-extraction technique. Materials Science and Engineering A. 2015;**636**:157

[16] Liu Y, Zhang X, Xing D, Qian M, Shen H, Wang H, Liu J, Sun J. Shape memory effects of $Ni_{49.7}Mn_{25.0}Ga_{19.8}Fe_{5.5}$ microwires prepared by rapid solidification. Physica Status Solidi (A). 2014;**211**:2532

[17] Zhang X, Qian M, Zhang Z, Wei L, Geng L, Sun J. Magnetostructural coupling and magnetocaloric effect in Ni-Mn-Ga-Cu microwires. Applied Physics Letters. 2016;**108**:52401

[18] Zhang H, Qian M, Zhang X, Jiang S, Wei L, Xing D, Sun J, Geng L. Magnetocaloric effect of Ni-Fe-Mn-Sn microwires prepared by melt-extraction technique. Materials & Design. 2017;**114**:1

[19] Liu Y, Zhang X, Xing D, Shen H, Chen D, Liu J, Sun J. Magnetocaloric effect (MCE) in melt-extracted Ni-Mn-Ga-Fe Heusler microwires. Journal of Alloys and Compounds. 2014;**616**:184

[20] Kainuma R, Imano Y, Ito W, Sutou Y, Morito H, Okamoto S, Kitakami O, Oikawa K, Fujita A, Kanomata T, Ishida K. Magnetic-field-induced shape recovery by reverse phase transformation. Nature. 2006;**439**:957

[21] Liu J, Gottschall T, Skokov KP, Moore JD, Gutfleisch O. Giant magnetocaloric effect driven by structural transitions. Nature Materials. 2012;**11**:620

[22] Pasquale M, Sasso CP, Lewis LH, Giudici L, Lograsso T, Schlagel D. Magnetostructural transition and magnetocaloric effect in $Ni_{55}Mn_{20}Ga_{25}$ single crystals. Physical Review B. 2005;**72**:094435

[23] Li Z, Zhang Y, Sánchez-Valdés CF, Sánchez Llamazares JL, Esling C, Zhao X, Zuo L. Giant magnetocaloric effect in melt-spun Ni-Mn-Ga ribbons with magneto-multistructural transformation. Applied Physics Letters. 2014;**104**:44101

[24] Li Z, Xu K, Zhang Y, Tao C, Zheng D, Jing C. Two successive magneto-structural transformations and their relation to enhanced magnetocaloric effect for $Ni_{55.8}Mn_{18.1}Ga_{26.1}$ Heusler alloy. Scientific Report-UK. 2015;**5**:15143

[25] Vasil'Ev AN, Bozhko AD, Khovailo VV, Dikshtein IE, Shavrov VG, Buchelnikov VD, Matsumoto M, Suzuki S, Takagi T, Tani J. Structural and magnetic phase transitions in shape-memory alloys $Ni_{2+x}Mn_{1-x}Ga$. Physical Review B. 1999;**59**:1113

[26] Chernenko VA. Compositional instability of beta-phase in Ni-Mn-Ga alloys. Scripta Materialia. 1999;**40**:523

[27] Ullakko K, Ezer Y, Sozinov A, Kimmel G, Yakovenko P, Lindroos VK. Magnetic-field-induced strains in polycrystalline Ni-Mn-Ga at room temperature. Scripta Materialia. 2001;**44**:475

[28] Murray SJ, Farinelli M, Kantner C, Huang JK, Allen SM, O'Handley RC. Field-induced strain under load in Ni-Mn-Ga magnetic shape memory materials. Journal of Applied Physics. 1998;**83**:7297

[29] Jin X, Marioni M, Bono D, Allen SM, O Handley RC, Hsu TY. Empirical mapping of Ni-Mn-Ga properties with composition and valence electron concentration. Journal of Applied Physics. 2002;**91**:8222

[30] Wu SK, Yang ST. Effect of composition on transformation temperatures of Ni-Mn-Ga shape memory alloys. Materials Letters. 2003;**57**:4291

[31] Segui C, Cesari E, Pons J, Chernenko V. Internal friction behaviour of Ni-Mn-Ga. Materials Science and Engineering A. 2004;**370**:481

[32] Chernenko VA, Pons J, Segu C, Cesari E. Premartensitic phenomena and other phase transformations in Ni-Mn-Ga alloys studied by dynamical mechanical analysis and electron diffraction. Acta Materialia. **2002**;50:53

[33] Ayuela A, Enkovaara J, Ullakko K, Nieminen RM. Structural properties of magnetic Heusler alloys. Journal of Physics: Condensed Matter. 1999;**11**:2017

[34] Jiang C, Wang J, Li P, Jia A, Xu H. Search for transformation from paramagnetic martensite to ferromagnetic austenite: NiMnGaCu alloys. Applied Physics Letters. 2009;**95**:12501

[35] Zhang XX, Witherspoon C, Mullner P, Dunand DC. Effect of pore architecture on magnetic-field-induced strain in polycrystalline Ni-Mn-Ga. Acta Materialia. 2011;**59**:2229

[36] Conde Y, Despois JF, Goodall R, Marmottant A, Salvo L, San Marchi C, Mortensen A. Replication processing of highly porous materials. Advanced Engineering Materials. 2006;**8**:795

[37] Brothers AH, Scheunemann R, DeFouw JD, Dunand DC. Processing and structure of open-celled amorphous metal foams. Scripta Materialia. 2005;**52**:335

[38] Peng H, Qin F, Phan M. Ferromagnetic Microwire Composites. DE: Springer Verlag; 2016

[39] Zhang Y, Li M, Wang YD, Lin JP, Dahmen KA, Wang ZL, Liaw PK. Superelasticity and serration behavior in small-sized NiMnGa alloys. Advanced Engineering Materials. 2014;**16**:955

[40] Zheng P, Kucza NJ, Patrick CL, Müllner P, Dunand DC. Mechanical and magnetic behavior of oligocrystalline Ni-Mn-Ga microwires. Journal of Alloys and Compounds. 2015;**624**:226

[41] Yan A, Muller KH, Gutfleisch O. Structure and magnetic entropy change of melt-spun $LaFe_{11.57}Si_{1.43}$ ribbons. Journal of Applied Physics. 2005;**97**:4494

[42] Planes A, Obrado E, GonzalezComas A, Manosa L. Premartensitic transition driven by magnetoelastic interaction in bcc ferromagnetic Ni_2MnGa. Physical Review Letters. 1997;**79**:3926

[43] Zheludev A, Shapiro SM, Wochner P, Tanner LE. Precursor effects and premartensitic transformation in Ni_2MnGa. Physical Review B. 1996;**54**:15045

[44] Brown PJ, Crangle J, Kanomata T, Matsmuoto M, Neumann KU, Ouladdiaf B, Ziebeck K. The crystal structure and phase transitions of the magnetic shape memory compound Ni_2MnGa. Journal of Physics: Condensed Matter. 2002;**14**:10159

[45] Chernenko VA, L'Vov V, Pons J, Cesari E. Superelasticity in high-temperature Ni-Mn-Ga alloys. Journal of Applied Physics. 2003;**93**:2394

[46] Mullner P, Mukherji D, Aguirre M, Erni R, Kostorz G. Micromechanics of magnetic-field-induced twin-boundary motion in Ni-Mn-Ga magnetic shape-memory alloys. Solid-Solid Phase Transformations in Inorganic Material. 2005;**2**:171

[47] Nespoli A, Besseghini S, Pittaccio S, Villa E, Viscuso S. The high potential of shape memory alloys in developing miniature mechanical devices: A review on shape memory alloy mini-actuators. Sensors and Actuators A: Physical. 2010;**158**:149

[48] Li Y, Jiang C, Liang T, Ma Y, Xu H. Martensitic transformation and magnetization of Ni-Fe-Ga ferromagnetic shape memory alloys. Scripta Materialia. 2003;**48**:1255

[49] Han ZD, Wang DH, Zhang CL, Xuan HC, Zhang JR, Gu BX, Du YW. The martensitic transformation and the magnetocaloric effect in $Ni_{50-x}Mn_{38+x}In_{12}$ alloys. Solid State Communications. 2008;**146**:124

[50] Liu Z, Wang H, Yu S, Dai X, Chen J, Wu G, Liu Y. Phase equilibrium of ferromagnetic shape memory alloy $Co_{39}Ni_{33}Al_{28}$. Scripta Materialia. 2006;**54**:1299

[51] Rolfs K, Chmielus M, Wimpory RC, Mecklenburg A, Müllner P, Schneider R. Double twinning in Ni-Mn-Ga-Co. Acta Materialia. 2010;**58**:2646

[52] Guldbakke JM, Chmielus M, Rolfs K, Schneider R, Müllner P, Raatz A. Magnetic, mechanical and fatigue properties of a $Ni_{45.4}Mn_{29.1}Ga_{21.6}Fe_{3.9}$ single crystal. Scripta Materialia. 2010;**62**:875

[53] Gao L, Dong GF, Gao ZY, Cai W. Effect of Dy addition on mechanical and magnetic properties of Mn-rich Ni-Mn-Ga ferromagnetic shape memory alloys. Journal of Alloys and Compounds. 2012;**520**:281

[54] Sozinov A, Likhachev AA, Lanska N, Ullakko K. Giant magnetic-field-induced strain in NiMnGa seven-layered martensitic phase. Applied Physics Letters. 2002;**80**:1746

[55] Cai PY, Feng SS, Chen WP, Xue SX, Li ZG, Zhou Y, Wang HB, Wang GP. Magnetic entropy change and magnetic-field-induced strain in polycrystalline $Ni_{47}Mn_{32}Ga_{21}$ alloy. Acta Physica Sinica-Chinese Edition. 2011;**60**:623

[56] Guo SH, Zhang YH, Li JL, Qi Y, Quan BY, Wang XL. Magnetic-field-induced strains of bonded Ni-Mn-Ga melt-spun ribbons. Chinese Physics Letters. 2006;**23**:227

[57] Gaitzsch U, Potschke M, Roth S, Rellinghaus B, Schultz L. Mechanical training of polycrystalline 7M $Ni_{50}Mn_{30}Ga_{20}$ magnetic shape memory alloy. Scripta Materialia. 2007;**57**:493

[58] Gaitzsch U, Potschke M, Roth S, Rellinghaus B, Schultz L. A 1% magnetostrain in polycrystalline 5M Ni-Mn-Ga. Acta Materialia. 2009;**57**:365

[59] Gaitzsch U, Romberg J, Potschke M, Roth S, Mullner P. Stable magnetic-field-induced strain above 1% in polycrystalline Ni-Mn-Ga. Scripta Materialia. 2011;**65**:679

[60] Potschke M, Weiss S, Gaitzsch U, Cong DY, Hurrich C, Roth S, Schultz L. Magnetically resettable 0.16% free strain in polycrystalline Ni-Mn-Ga plates. Scripta Materialia. 2010;**63**:383

[61] Ham-Su R, Healey JP, Underhill RS, Farrell SP, Cheng LM, Hyatt C, Chen J, Gharghouri MA. Vibration damping material employing magnetic shape memory alloys. Aerospace Materials and Manufacturing: Development, Testing, and Life Cycle Issues - Honoring William Wallace. Canadian Institute of Mining, Metallurgy and Petroleum, Montreal, QC; 2004. p. 335

[62] Wang X, Dapino MJ. Behavior of nimnga under dynamic magnetic fields considering magnetic diffusion and eddy current power loss. Proceedings of the ASME International Mechanical Engineering Congress and Exposition 2007, Vol. 10, Pts A and B: Mechanics of Solids and Structures; 2008. p 381

[63] Ganor Y, Shilo D, Shield TW, James RD. Breaching the work output limitation of ferromagnetic shape memory alloys. Applied Physics Letters. 2008;**93**:4301

[64] Scheerbaum N, Lai YW, Leisegang T, Thomas M, Liu J, Khlopkov K, McCord J, Fähler S, Träger R, Meyer DC. Constraint-dependent twin variant distribution in Ni_2MnGa single crystal, polycrystals and thin film: An EBSD study. Acta Materialia. 2010;**58**:4629

[65] Chen Y, Schuh CA. Size effects in shape memory alloy microwires. Acta Materialia. 2011;**59**:537

[66] Qian MF, Zhang XX, Wei LS, Geng L, Peng HX. Structural, Magnetic and mechanical properties of oligocrystalline Ni-Mn-Ga shape memory microwires. Materials Today: Proceedings. 2015;**2**:S577

[67] Caron L, Ou ZQ, Nguyen TT, Thanh DTC, Tegus O, Bruck E. On the determination of the magnetic entropy change in materials with first-order transitions. Journal of Magnetism and Magnetic Materials. 2009;**321**:3559

[68] Fujieda S, Fujita A, Fukamichi K. Reduction of hysteresis loss and large magnetocaloric effects in substituted compounds of itinerant-electron metamagnets $La(Fe_xSi_{1-x})_{13}$. Journal of Magnetism and Magnetic Materials. 2009;**321**:3567

[69] Zhao J, Shen J, Hu F, Li Y, Sun J, Shen B. Reduction of magnetic hysteresis loss in $La_{0.5}Pr_{0.5}Fe_{11.4}Si_{1.6}H_x$ hydrides with large magnetocaloric effects. Journal of Applied Physics. 2010;**107**:113911

[70] Shen J, Li Y, Sun J, Shen B. Effect of R substitution on magnetic properties and magnetocaloric effects of $La_{1-x}R_xFe_{11.5}Si_{1.5}$ compounds with R = Ce, Pr and Nd. Chinese Physics B. 2009;**18**:2058

[71] Pecharsky VK, Gschneidner KA. Giant magnetocaloric effect in $Gd_5(Si_2Ge_2)$. Physical Reviews Letters. 1997;**78**:4494

[72] Wada H, Tanabe Y. Giant magnetocaloric effect of $MnAs_{1-x}Sb_x$. Applied Physics Letters. 2001;**79**:3302

[73] Carvalho AMG, Coelho AA, von Ranke PJ, Alves CS. The isothermal variation of the entropy (Delta S-T) may be miscalculated from magnetization isotherms in some cases: MnAs and $Gd_5Ge_2Si_2$ compounds as examples. Journal of Alloys and Compounds. 2011;**509**:3452

[74] Sun NK, Liu F, Gao YB, Cai ZQ, Du BS, Xu SN, Si PZ. Effect of microstrain on the magnetism and magnetocaloric properties of $MnAs_{0.97}P_{0.03}$. Applied Physics Letters. 2012; **100**:112407

[75] Nguyen HD, Zhang L, Ou ZQ, Bruck E. Magnetoelastic coupling and magnetocaloric effect in hexagonal Mn-Fe-P-Si compounds. Scripta Materialia. 2012;**67**:975

[76] Yibole H, Guillou F, Zhang L, van Dijk NH, Bruck E. Direct measurement of the magnetocaloric effect in MnFe(P,X) (X = As, Ge, Si) materials. Journal of Physics D: Applied Physics. 2014;**47**:75002

[77] Manekar M, Roy SB. Reproducible room temperature giant magnetocaloric effect in Fe-Rh. Journal of Physics D: Applied Physics. 2008;**41**:192004

[78] Krenke T, Duman E, Acet M, Wassermann EF, Moya X, Manosa L, Planes A. Inverse magnetocaloric effect in ferromagnetic Ni-Mn-Sn alloys. Nature Materials. **2005**;4:450

[79] Krenke T, Duman E, Acet M, Moya X, Manosa L, Planes A. Effect of Co and Fe on the inverse magnetocaloric properties of Ni-Mn-Sn. Journal of Applied Physics. 2007; **102**:33903

[80] Gao B, Hu FX, Shen J, Wang J, Sun JR, Shen BG. Field-induced structural transition and the related magnetic entropy change in $Ni_{43}Mn_{43}Co_3Sn_{11}$ alloy. Journal of Magnetism and Magnetic Materials. 2009;**321**:2571

[81] Takeuchi AY, Guimaraes CE, Passamani EC, Larica C. Enhancement of magnetocaloric properties near room temperature in Ga-doped $Ni_{50}Mn_{34.5}In_{15.5}$ Heusler-type alloy. Journal of Applied Physics. 2012;**111**:3867

[82] Zhang Y, Zheng Q, Xia W, Zhang J, Du J, Yan A. Enhanced large magnetic entropy change and adiabatic temperature change of $Ni_{43}Mn_{46}Sn_{11}$ alloys by a rapid solidification method. Scripta Materialia. 2015;**104**:41

[83] Yan A, Mueller KH, Gutfleisch O. Magnetocaloric effect in $LaFe_{11.8-x}Co_xSi_{1.2}$ melt-spun ribbons. Journal of Alloys and Compounds. 2008;**450**:18

[84] Zhang X, Qian M, Miao S, Su R, Liu Y, Geng L, Sun J. Enhanced magnetic entropy change and working temperature interval in Ni-Mn-In-Co alloys. Journal of Alloys and Compounds. 2016;**656**:154

[85] Zhang Y, Zhang L, Zheng Q, Zheng X, Li M, Du J, Yan A. Enhanced magnetic refrigeration properties in Mn-rich Ni-Mn-Sn ribbons by optimal annealing. Scientific Reports-UK. 2015;**5**

[86] Dubenko I, Samanta T, Pathak AK, Kazakov A, Prudnikov V, Stadler S, Granovsky A, Zhukov A, Ali N. Magnetocaloric effect and multifunctional properties of Ni-Mn-based Heusler alloys. Journal of Magnetism and Magnetic Materials. 2012;**324**:3530

[87] Quetz A, Koshkid'Ko YS, Titov I, Rodionov I, Pandey S, Aryal A, Ibarra-Gaytan PJ, Prudnikov V, Granovsky A, Dubenko I, Samanta T, Cwik J, Sanchez Llamazares JL, Stadler S, Lahderanta E, Ali N. Giant reversible inverse magnetocaloric effects in $Ni_{50}Mn_{35}In_{15}$ Heusler alloys. Journal of Alloys and Compounds. 2016;**683**:139

[88] Dong JD, Yan AR, Liu J. Microstructure and magnetocaloric properties of melt-extracted La-Fe-Si microwires. Journal of Magnetism and Magnetic Materials. 2014;**357**:73

[89] Ilyn MI, Zhukova V, Santos JD, Sánchez ML, Prida VM, Hernando B, Larin V, González J, Tishin AM, Zhukov A. Magnetocaloric effect in nanogranular glass coated microwires. Physica Status Solidi (A). 2008;**205**:1378

[90] Aguilar-Ortiz CO, Soto-Parra D, Álvarez-Alonso P, Lázpita P, Salazar D, Castillo-Villa PO, Flores-Zúñiga H, Chernenko VA. Influence of Fe doping and magnetic field on martensitic transition in Ni-Mn-Sn melt-spun ribbons. Acta Materialia. 2016;**107**:9

[91] Yuzuak E, Dincer I, Elerman Y, Auge A, Teichert N, Hutten A. Inverse magnetocaloric effect of epitaxial Ni-Mn-Sn thin films. Applied Physics Letters. 2013;**103**:222403

[92] Recarte V, Perez-Landazabal JI, Sanchez-Alarcos V, Chernenko VA, Ohtsuka M. Magnetocaloric effect linked to the martensitic transformation in sputter-deposited Ni-Mn-Ga thin films. Applied Physics Letters. 2009;**95**

[93] Hu F, Shen B, Sun J. Magnetic entropy change involving martensitic transition in NiMn-based Heusler alloys. Chinese Physics B. 2013;**22**:037505

[94] Duan J, Huang P, Zhang H, Long Y, Wu G, Ye R, Chang Y, Wan F. Negative and positive magnetocaloric effect in Ni-Fe-Mn-Ga alloy. Journal of Magnetism and Magnetic Materials. 2007;**309**:96

[95] Varga R, Ryba T, Vargova Z, Saksl K, Zhukova V, Zhukov A. Magnetic and structural properties of Ni-Mn-Ga Heusler-type microwires. Scripta Materialia. 2011;**65**:703

[96] Srivastava SK, Srivastava VK, Chatterjee R. Magnetocaloric properties of $Ni_{2.29}Mn_{0.89}Ga_{0.82}$ alloy. Solid State Communications. 2012;**152**:372

[97] Stadler S, Khan M, Mitchell J, Ali N, Gomes AM, Dubenko I, Takeuchi AY, Guimarães AP. Magnetocaloric properties of $Ni_2Mn_{1-x}Cu_xGa$. Applied Physics Letters. 2006;**88**:192511

[98] Huang C, Wang Y, Tang Z, Liao X, Yang S, Song X. Influence of atomic ordering on elastocaloric and magnetocaloric effects of a Ni-Cu-Mn-Ga ferromagnetic shape memory alloy. Journal of Alloys and Compounds. 2015;**630**:244

[99] Duan JF, Long Y, Bao B, Zhang H, Ye RC, Chang YQ, Wan FR, Wu GH. Experimental and theoretical investigations of the magnetocaloric effect of $Ni_{2.15}Mn_{0.85-x}Cu_xGa$ (x = 0.05, 0.07) alloys. Journal of Applied Physics. 2008;**103**

[100] Dan'Kov SY, Tishin AM, Pecharsky VK, Gschneidner KA. Magnetic phase transitions and the magnetothermal properties of gadolinium. Physical Review B. 1998;**57**:3478

[101] Gutfleisch O, Yan A, Müller KH. Large magnetocaloric effect in melt-spun $LaFe_{13-x}Si_x$. Journal of Applied Physics. 2005;**97**:10M

[102] Xu HB, Ma YQ, Jiang CB. A high-temperature shape-memory alloy $Ni_{54}Mn_{25}Ga_{21}$. Applied Physics Letters. 2003;**82**:3206

[103] Xin Y, Li Y, Chai L, Xu HB. Shape memory characteristics of dual-phase Ni-Mn-Ga based high temperature shape memory alloys. Scripta Materialia. 2007;**57**:599

[104] Glavatskyy I, Glavatska N, Soderberg O, Hannula SP, Hoffmann JU. Transformation temperatures and magnetoplasticity of Ni-Mn-Ga alloyed with Si, In, Co or Fe. Scripta Materialia. 2006;54:1891

[105] Glavatskyy I, Glavatska N, Dobrinsky A, Hoffmann JU, Sorberg O, Hannula SP. Crystal structure and high-temperature magnetoplasticity in the new Ni-Mn-Ga-Cu magnetic shape memory alloys. Scripta Materialia. 2007;**56**:565

[106] Ma YQ, Yang SY, Wang CP, Liu XJ. Tensile characteristics and shape memory effect of $Ni_{56}Mn_{21}Co_4Ga_{19}$ high-temperature shape memory alloy. Scripta Materialia. 2008;**58**:918

[107] Soto D, Hernandez FA, Flores-Zuniga H, Moya X, Manosa L, Planes A, Aksoy S, Acet M, Krenke T. Phase diagram of Fe-doped Ni-Mn-Ga ferromagnetic shape-memory alloys. Physical Review B. 2008;**77**:1

[108] Soto-Parra DE, Vives E, Gonzalez-Alonso D, Manosa L, Planes A, Romero R, Matutes-Aquino JA, Ochoa-Gamboa RA, Flores-Zuniga H. Stress- and magnetic field-induced entropy changes in Fe-doped Ni-Mn-Ga shape-memory alloys. Applied Physics Letters. 2010;**96**

[109] Magnetic shape memory actuators. http://www.themsmnet.net/devices.html

[110] Wilson SA, Jourdain RPJ, Zhang Q, Dorey RA, Bowen CR, Willander M, Wahab QU, Willander M, Al-hilli SM, Nur O, Quandt E, Johansson C, Pagounis E, Kohl M, Matovic J, Samel B, van der Wijngaart W, Jager EWH, Carlsson D, Djinovic Z, Wegener M, Moldovan C, Iosub R, Abad E, Wendlandt M, Rusu C, Persson K. New materials for micro-scale sensors and actuators. Materials Science and Engineering: R: Reports. 2007;**56**:1

[111] Boise State Micro-Pump Aids Neurological Research. 2014. https://news.boisestate.edu/update/2014/09/24/micro-pump-developed-boise-state-aids-neurological-research-england/

[112] Franco V, Blazquez JS, Ingale B, Conde A. The magnetocaloric effect and magnetic refrigeration near room temperature: Materials and models. In: Clarke DR, editor. Annual Review of Materials Research, vol. 42. Palo Alto: Annual Reviews; 2012. p. 305

[113] Krautz M, Skokov K, Gottschall T, Teixeira CS, Waske A, Liu J, Schultz L, Gutfleisch O. Systematic investigation of Mn substituted La(Fe,Si)(13) alloys and their hydrides for room-temperature magnetocaloric application. Journal of Alloys and Compounds. 2014;**598**:27